Student thesis series INES nr 501

Exploring methods for detecting maize plant density using Structure-from-Motion point clouds

Tom Albin Tveitan Käppi

2020
Department of
Physical Geography and Ecosystem Science
Lund University
Sölvegatan 12
S-223 62 Lund
Sweden

Tom Albin Tveitan Käppi (2020).
Exploring methods for detecting maize plant density using Structure-from-Motion point clouds
Utforskande av metoder för att bestämma planttäthet hos majs med fotogrammetriska punktmoln
Master degree thesis, 30 credits in *Geomatics*
Department of Physical Geography and Ecosystem Science, Lund University

Level: Master of Science (MSc)
Course duration: January 2019 until *June* 2019

Disclaimer

Exploring methods for detecting maize plant density using Structure-from-Motion point clouds

---

Tom Albin Tveitan Käppi

Master thesis, 30 credits, in *Geomatics**

Supervisors:
Per-Ola Olsson
Department of Physical Geography and Ecosystem Science
Lund University

Ola Hall
Department of Human Geography
Lund University

Exam committee:
Jonas Ardö
Lars Eklundh
Department of Physical Geography and Ecosystem Science
Lund University

Acknowledgements

I am thankful towards my supervisors Per-Ola Olsson and Ola Hall for providing me with guidance and technical support throughout the writing of my thesis. I would also like to thank my fellow students and friends that have taken the time to provide feedback on this thesis, our discussions have been invaluable.

Abstract

The population of earth is projected to increase the coming decades. This can pose problems of food security and demands a more productive food sector as well as methods of assessing food productivity in relation to demand. Crop monitoring with remote sensing can guide precision farming used for sustainable intensification of agriculture, as well as contribute to yield forecasting models useful for food security assessments. Developing low cost methods for crop monitoring can support sustainable intensification of agriculture and provide useful yield information in advance. A relatively recent development in remote sensing technology is the possibility of modelling crops in 3D through Structure-from-Motion (SfM) technology using imagery gathered from Unmanned Aerial Vehicles (UAVs). This study therefore aimed to explore the use of SfM technology to determine maize plant density, a parameter related to plant yield. The study explored two methods based on point clouds generated from UAV imagery to determine the density of maize plants. The first method employed a simple linear regression to explore a potential relation between a metric of variations in maize canopy elevation and maize plant density. A relation between the variables was indicated, motivating further testing of this method. However, the method proved to be vulnerable to heterogeneous plant distributions within the sample areas. This outlined the importance of the sample area size in relation to the spatial distribution of the plants modelled. A danger of misidentifying bare areas as areas of high plant density was also discovered, indicating that large areas without plants should be excluded before applying the method. The second method aimed at delineating individual maize plants through generating elevation contours on a triangulation of a point cloud. By querying the contours on height and length, contours would ideally be placed at the location of maize plants. The results showed low accuracy in relation to available validation data, possibly due to the complex geometry of the plants. Furthermore, the presence of blur in the imagery as well as the use of suboptimal UAV flight planning for 3D modelling purposes might have influenced results of both methods.

Keywords: Geography, Ecosystem Analysis, Maize plant density, Structure-from-Motion, Unmanned Aerial Vehicles (UAV)

Sammanfattning

Jordens befolkning förväntas öka de kommande årtiondena. Detta kan skapa osäkerhet kring livsmedelsförsörjning och kräver en mer produktiv livsmedelssektor samt metoder för att bedöma tillgång på livsmedel i förhållande till efterfrågan. Utvecklandet av lågkostnadsmetoder för övervakning av grödor kan stödja en hållbar intensifiering av jordbruket och tillhandahålla användbar information kring skörd i förväg. En relativt ny utveckling inom fjärranalystekniken är möjligheten att modellera en grödas krontak i 3D genom Structure-from-Motion (SfM) teknologi. Denna teknik använder överlappande bilder för att skapa ett tredimensionellt punktmoln genom fotogrammetriska principer. Denna studie syftade därför till att undersöka användningen av SfM-teknik för att bestämma majsens planttäthet, en skörd-relaterad plantparameter. Studien undersökte två metoder baserade på punktmoln som genererades från drönarbilder för att bestämma tätheten av majsplantor. I den första metoden användes en enkel linjär regression för att utforska en potentiell relation mellan ett mått på variationer i höjd på punkter i punkmolnet och majsens planttäthet. Ett svagt samband hittades, men metoden visade sig vara sårbar för heterogena plantfördelningar inom provområdena. Detta påvisade vikten av provområdets storlek i förhållande till den spatiala fördelningen av de modellerade plantorna. En risk för felidentifiering av större områden utan plantor som områden med hög växtdensitet upptäcktes också, vilket tyder på att stora ytor utan plantor bör uteslutas innan man tillämpar metoden. Den andra metoden syftade till att avgränsa enskilda majsplantor genom att generera höjdkonturer på kontinuerliga ytmodeller baserade på punktmoln. Genom att sortera ut konturerna på höjd och längd, skulle konturerna placeras på majsplantornas position. Resultaten hade låg exakthet i förhållande till valideringsdata, potentiellt på grund av svårigheten att applicera metoden på objekt med så komplex geometri som majsplantor. Oskarpa drönarbilder och suboptimal UAV-flygplanering för 3D-modelleringsändamål kan också ha påverkat resultaten från båda metoder.

Nyckelord: Geografi, Ekosystemvetenskap, Planttäthet, Majs, Structure-from-Motion, Unmanned Aerial Vehicles (UAV)

Contents

1 Introduction

The population of Earth is growing and is projected to become home to around 9.8 billion people by 2050, with the highest population increase expected on the African continent (United Nations 2017). A growing population means higher pressure on Earth's resources, not least when it comes to food production. At the same time there is increased competition for land that can be used for food production due to anthropogenic processes such as urbanization and biofuel production (Molony and Smith 2017; van Vliet et al. 2017) and land degradation processes (Bai et al. 2008; Webb et al. 2017). This means that efforts need to be focused on making the most of the cultivated land that is currently available by improving the use of inputs such as fertilizer, irrigation and pesticides in a resource sustainable manner (Nellemann and MacDevette 2009; Pretty and Bharucha 2014; van Ittersum et al. 2016). By measuring the spatial and temporal variability in cropland with regards to for example crop stress, soil moisture, soil nitrogen content, incidence of weeds and microclimate, agricultural inputs can be added where most needed. This method of micromanaging agriculture is known as precision agriculture, and can reduce excessive use of agricultural inputs, leading to increased profitability for farmers and a decrease in environmental consequences such as the pollution of water sources and greenhouse gas emissions due to nitrogen leakage (Daughtry et al. 2000; Mensah et al. 2018). In addition to improving farm productivity, the ability of making yield forecasts is also of importance to assess food productivity in relation to food demand.

Satellite remote sensing is a well-established method for measuring plant biophysical parameters of interest in agriculture, and is therefore an important tool for precision agriculture and yield forecasting. For example, the relationship between spectral reflectance and the chlorophyll content of the plant (Yoder and Pettigrew-Crosby 1995) is used to detect spatial variations in crop stress and ultimately where to focus agricultural inputs (Mulla 2013). In more recent years, Unmanned Aerial Vehicles (UAV) with mounted cameras has proven valuable as a platform for gathering information on plant health status. UAVs can be advantageous in comparison to satellites for precision agriculture purposes, since they provide the possibility of gathering very high resolution data at almost any desired time, while being less restricted by atmospheric disturbances such as cloud cover (Hunt and Daughtry 2018).

In addition to measuring spectral properties of a field, UAVs also offer a new low-cost platform for photogrammetric measurements of objects at close range. This allows for capturing the geometry of plants in three dimensions, enabling the farmer to get information such as plant height variations within a field. Using photogrammetry to estimate heights of complex surfaces, such as cropland, requires a very high resolution and a large overlap between images. While high-resolution data is increasingly available from satellite imagery, the financial cost and low temporal resolution make it less suitable for photogrammetric reconstructions of farmer's fields (Li et al. 2016). The geometry of the field can be reconstructed from a set of overlapping images using the Structure-from-Motion (SfM) technique. The technique draws on the principles of photogrammetry to derive the 3D

coordinates of features in the images as points, resulting in a three dimensional (3D) point cloud (Westoby et al. 2012). This point cloud models the structure of the crop canopy, and the distribution of points in the point cloud can then be used to derive important yield-related information about the plants.

The use of such SfM point clouds in crop remote sensing has thus far been centered on creating crop height models (Bendig et al. 2013; De Souza et al. 2017; Han et al. 2018), often to investigate correlations between plant height and grain yield or biomass (Michez et al. 2018; Näsi et al. 2018). Many of these studies have also been conducted on experimental plots, and have therefore not taken into account complexities often associated with remote sensing of smallholder farms, such as small and fragmented fields and greater heterogeneity of topography and management practices (Delrue et al. 2013; Lambert et al. 2018).

Although plant height is of great interest in precision agriculture, other plant components of interest might also be derived from SfM point clouds, such as plant density. Maize plant density is an important factor influencing yield as it is related to the plants nutrient uptake (Ciampitti and Vyn 2011; Assefa et al. 2018), as well as water use efficiency (Ogola et al. 2005; Lamm et al. 2009). If the optimal plant density of a farmer's field is known, knowledge on the actual plant density can then potentially be used to informer better farm management. Furthermore, since plant density is considered a key factor influencing yield, the knowledge of plant density can contribute to models used for yield forecasting (Van Ittersum et al. 2013). Yield forecasting can in turn provide knowledge in advance of an emerging food crisis, giving households and government much needed time for taking decisions (Delincé 2017). Knowledge on maize plant density might therefore be beneficial for both yield forecasting and precision agriculture purposes. While the Structure-from-Motion technology has potential as a new low-cost method to monitor crops (Zhang and Kovacs 2012), the detection of maize plant density with methods based on SfM point clouds is scarcely researched, and has not knowingly been studied in the context of smallholder maize fields in Sub-Saharan Africa. This motivates exploratory research in this field, and also means the study cannot draw heavily on previously researched methods used for the same purpose. This study should therefore be considered highly exploratory, and its results considered indicative of the methods potential rather than conclusive.

The data for this study is collected from maize fields in Ghana, and comprises a number of small-sized, rain-fed maize fields. This is a common agricultural scenario in many parts of Sub-Saharan Africa, and successful remote sensing of plant characteristics in this context might provide useful insights for precision agriculture and yield forecasting applications in similar environments. The UAV imagery for this research was gathered with a consumer grade Red-Green-Blue (RGB) camera and the results of the study might therefore also provide valuable insights into the viability of using SfM point clouds created with affordable consumer grade equipment.

1.1 Aim and research questions

Maize plant density is a plant parameter related to maize yield. However, the use of SfM point clouds to determine maize plant density is thus far scarcely researched. The aim of this study is therefore to explore whether maize plant density can be estimated using SfM point clouds produced from consumer grade UAV imagery taken at an altitude of approximately 100 m above ground level. Two methods are explored, where the first method attempts to provide a measure of maize plant density using spatial variations in point heights in a SfM point cloud. The second method aims to estimate maize plant density using elevation contours of the SfM point cloud to locate individual maize plants. The following research questions (RQ) have been formulated to meet the aim:

RQ1: Is it possible to estimate maize plant density using spatial variations in point heights in a maize canopy modelled by Structure-from-Motion technology?

- Is there an optimal cell size to capture point height variations for estimating maize plant density?

RQ2: Is it possible to identify individual maize plants using elevation contours created from SfM point clouds?

2 Background

2.1 Crop monitoring with remote sensing

Remote sensing of crops is a broad field that can encompass many techniques and spatial and temporal scales. On a coarse spatio-temporal scale, remote sensing of crops can involve measuring phenological stages of the crops from bud break to senescence from the spectral response of vegetation measured by multispectral satellite sensors. The spectral reflectance for some wavelengths varies largely in relation to the chlorophyll content of the vegetation. Monitoring of vegetation is often done with radiometric indices optimized for this purpose, where the most commonly used is the Normalized Difference Vegetation Index (NDVI) (Rouse et al. 1973). The NDVI and other similar vegetation indices (VIs) utilize the large difference in spectral reflectance between the red visible light and the near infrared (NIR) wavelengths for vegetation. This allows for the discrimination as well as vigor estimation of vegetation and can be used to provide information on the length and magnitude of crop growth in that season (Dominique et al. 2016; Madigan et al. 2018).

Furthermore, satellite imagery can also be used to monitor crops on a higher spatio-temporal scale, allowing the gathering of information used within a growing season and for local yield forecasting. However, current free-to-use satellite imagery has too low image cell size for distinguishing intra-field crop stress variabilities on a detailed level, especially in contexts characterized by high fragmentation of fields and patchy, small clusters of vegetation (Vaccari et al. 2015) as in the case of this study. While commercial satellite data with high temporal and spatial resolution and multi-spectral sensors exists, the data can be relatively expensive for large scale use. Conversely, UAVs can produce high resolution aerial imagery continuously throughout a growing season for a relatively low cost in comparison to commercially available high resolution satellite imagery (Xue and Su 2017).

Applications of UAVs for crop monitoring include the use of VIs derived from UAV imagery for yield estimations. A study by Wahab et al. (2018) used a vegetation index similar to NDVI from UAV imagery for estimating variabilities in maize vigor and yield in smallholder maize plots. The study compared the final yield with visual estimations of crop vigor as well as in-field leaf-chlorophyll measurements during the growing season and concluded that the UAV derived vegetation index did comparatively better in predicting yields than the two in-field methods. Other studies explored UAV derived VIs for yield predictions in for example rice (Zhou et al. 2017; Duan et al. 2019) and wheat (Du and Noguchi 2017; Marino and Alvino 2019). Previous studies have also created crop height models with SfM from UAV imagery or used UAV borne LiDAR for crop monitoring purposes (Bendig et al. 2013; De Souza et al. 2017). A combination of UAV derived VIs and crop height models for yield prediction have also been previously explored (Geipel et al. 2014; Bendig et al. 2015; Maresma et al. 2016). While plant density is another important plant parameter related to yield, considerably fewer studies have been focused on the determination of plant density through UAV remote sensing.

2.2 Maize plant density and crop yield

One of the important yield related factors in maize is the distance at which the maize plants are growing. A study by Magaia et al. (2017) set in Mozambique investigated the relationship between fertilizer needs and maize plant density under both rain-fed and irrigated scenarios and came to the conclusion that grain yield varied with different maize densities. Plots with different plant densities responded differently to increases in fertilizer and the amount of water the plants received throughout the season. Low density maize plots showed a lower response to the application of fertilizer than high density maize plots. The study also indicated that rain-fed maize is more sensitive to planting patterns than irrigated maize. Another study that investigated the relationship between plant density, nitrogen uptake and plant biomass showed that higher densities of maize plants had positive effects on the plants efficiency in utilizing the added nitrogen (Ciampitti and Vyn 2011). In addition, a study by Yan et al. (2017) found that too high maize plant densities can result in reduced yields due to increased competition for resources between plants.

While many studies show that maize plant density is an important yield related factor, the optimal density of the maize plant varies. This is due to the fact that the optimal density is highly dependent on the plant breed and local environment of the crop, as outlined by Sangoi (2001). Variables such as the local soil conditions can for example influence the ability of the plant to make use of added nitrogen (Kihara et al. 2016; Solomon et al. 2017). However, if the appropriate plant density for a region is known, information on actual plant density used by farmers can help improve general management practices among farmers in the region.

While fertilizer is recommended to be added 4-6 weeks after planting (WAP) in Ghana (Adu et al. 2014), the methods explored in this study attempts to determine the maize density of plants 8 WAP. However, some studies have indicated that application of fertilizer in later stages of maize growth can also benefit yields (Silva et al. 2006; Zheng et al. 2018), meaning knowledge of maize density in later stages can potentially also be used to influence management practices within a growing season. Furthermore, as plant density is one of the key attributes of crop yield models, knowledge on plant density can potentially be used to improve local yield forecasts (Delincé 2017).

2.3 UAVs for maize plant density detection

The number and density of maize plants can be determined by walking through the field and manually counting the plants. Similar to the estimation of crop vigor visually or with handheld instruments, this is a strenuous and time-consuming task (Wahab et al. 2018) and calls for more efficient methods for determining plant density. UAV based methods of remote sensing have the potential of determining maize plant density in a more time and cost-efficient manner by gathering timely, high resolution data and through the possibility of adjusting flight height and sensor type for different aims (Gnädinger and Schmidhalter 2017; Varela et al. 2018).

Existing research aimed at determining maize plants density from UAV imagery have utilized image-based classification methods as well as two dimensional geometric descriptors. A study by Hall et al. (2018) on the same maize fields used in this study utilized object oriented image classification based on spectral values and texture to isolate single maize plant objects. Within these objects the centroid was determined to represent the location of the maize plant. The method overestimated the plant count by approximately 15%. Another recent study successfully detected individual maize plants in an early growth stage from ultra-high resolution UAV imagery (2.4mm ground sample distance) by training a decision tree classifier with a set of geometric descriptors of maize plants and weeds respectively (Varela et al. 2018).

However, since methods based on spectral values are two dimensional, overlapping plants can be hard to distinguish from each other. Similarly, distinguishing weeds from crops spectrally also pose a problem, given their often similar spectral signatures (Gnädinger and Schmidhalter 2017; Varela et al. 2018). Point cloud based methods have the possible advantage of distinguishing crops from low growing weeds, as well as from other overlapping crop plants by considering also the height difference between the plants.

UAVs can be used to create 3D point clouds of crops using either mounted Light Detection And Ranging (LIDAR) equipment or the SfM technique based on overlapping RGB imagery. SfM technology and LIDAR both produces 3D point clouds, but since the underlying technologies are different, the point clouds differ in their characteristics. LIDAR measures the time it takes for an emitted laser pulse to be reflected back to determine a point position, and can give several returns from one pulse since the laser beam can penetrate the canopy. These measurements results in a highly accurate 3D point cloud, where many layers below the canopy as well as the ground below it can be modelled. A SfM point cloud is however created from overlapping imagery, and so can only model the upper canopy as visible in the images from above (Wallace et al. 2016).

Several studies using LIDAR technology for estimating maize plant density exists. However, these studies have mostly used high-end ground-based LIDAR equipment (Höfle 2014), and often aimed to make highly detailed models of maize for phenotyping purposes (Shi et al. 2015; Qiu et al. 2019). UAV-borne LIDAR based methods for the detection maize plant density is on the other hand not knowingly researched. Several studies using UAV-borne LIDAR for detecting individual plants exist, but have mainly focused on the detection of individual trees for purposes of forestry inventory. These methods have for example utilized density-based clustering algorithms that are based on the Euclidean distance between points, such as the Mean Shift algorithm. This algorithm iteratively moves points into local clusters, where every point moves towards the local densest cluster of points until a number of points are left that represent the centers of each cluster (Yizong Cheng 2002). Studies that have utilized this type of clustering algorithms for segmentation of individual trees have achieved high accuracies (Hu et al. 2017; Chen et al. 2018). However, while measuring plant density is possible from LIDAR point clouds, the LIDAR equipment can be expensive in comparison to SfM technology that requires only a consumer grade RGB camera for 3D model creation.

Thus far, many studies modelling crops with SfM technology have been focused on modelling plant height and detecting height variabilities within cropland. A common aim has been to explore relations between height and above ground biomass to make yield predictions, often by combining crop height data with vegetation indices such as NDVI (Bendig et al. 2015; Li et al. 2016; Han et al. 2018; Michez et al. 2018). The measuring of plant density directly from SfM point clouds are on the other hand scarcely researched.

However, apart from providing information on the canopy height, SfM point clouds can also be used to derive information about the structure of a canopy. Simple metrics of canopy structure, such as the standard deviation of point height in an area, can then be used to derive information related to the plants geometry and spatial distribution. Studies have for example found correlations between metrics of canopy structure and Leaf Area Index for maize plots (Li et al. 2017) and vineyards (Mathews and Jensen 2013). Since the spatial distribution of plants influences the canopy structure, such metrics could potentially also be used to estimate plant density as attempted in the first method explored in this study. Furthermore, if the maize plants can be distinguished from each other through their height, plant density might be estimated by delineating individual maize plants as attempted in the second method explored in this study.

Since methods for detecting plant density for maize or similar crops directly from a SfM point cloud is not knowingly researched, this study cannot be put into relation to earlier research using similar methods. Rather than building on previous research and providing conclusive results, the study instead aims to explore two new methods based on SfM technology in the hope to provide new ideas for measuring maize plant density.

2.4 Structure-from-Motion and point cloud quality

The SfM procedure from UAV imagery to point cloud can be split into three major steps. The initial step is the detection of individual image features that can be identified in several images. This feature identification is often achieved with a version of the Scale Invariant Feature Transform (SIFT) algorithm (Schonberger and Frahm 2016). The SIFT algorithm identifies distinct features in an image at different spatial scales and creates descriptive information about each of these features, or "keypoints" (Lowe 2004).

The second step is the bundle adjustment which computes a sparse 3D point cloud of the scene, by solving for the images orientation with the help of the SIFT derived keypoints in every image. The common keypoints are identified in different images. Lastly, the density of the point cloud is then commonly increased through Multi View Stereo techniques, resulting in a 3D product that can be used for subsequent analysis (Westoby et al. 2012).

Some commercial photogrammetry software such as Agisoft PhotoScan (Agisoft LLC 2018) incorporates all the steps from image feature identification to point cloud creation, using a workflow similar to that described above (Semyonov 2011). This makes it easy for the user to process their data without the need to combine different software. Simultaneously, the commercial nature of the software inhibits a thorough understanding of the underlying algorithms. This can prevent a user from fully grasping the nature of the results and potential

error sources. He et al. (2018) argue for the need of a transparent, open-source SfM method, especially for precision agriculture purposes, since the repetitive texture of crops makes the keypoint creation and feature matching between images highly error prone. Nevertheless, several empirical studies exist that examine the effect of various factors on the quality of a final SfM point cloud through experimental approaches.

Dandoi et al. (2015), for example, investigated the influence that different observation conditions had on the quality of a point cloud modelling a forest canopy structure. The observed parameters included point positioning accuracy, point cloud density and canopy penetration. These are all important parameters when modelling vegetation canopy structure, since they influence the horizontal and vertical accuracy of points as well as how well fine details are captured in the final point cloud. The observational conditions investigated included different light conditions and image overlap. Forward overlap was considered one of the most important factors influencing point cloud quality. The study showed that large forward overlap had a strong positive correlation to both point cloud density and to what extent the point cloud penetrated the canopy to the ground level. A 90% forward overlap penetrated all the way to the ground in vegetation gaps, while a 60% forward overlap reached approximately half way to the ground from the canopy. Furthermore, gathering imagery on cloudy days would produce images of lower contrast, while sunny days would produce shadows that obscured parts of the canopy. A specific light condition could therefore not be recommended.

De Souza et al. (2017) estimated the heights of sugar cane fields and simultaneously investigated the influence of flight directions on the generation of the point cloud. They concluded that height estimations within the same field varied with flight direction due to differences in radiometric properties of features at different camera angles. These effects, often caused by shading, could subsequently be mitigated by using cross-directional flights. Using cross directional flights made for a better crop height estimation, both due to larger overlap and less sensitivity to shading effects.

Furthermore, Sieberth et al. (2014) investigated the impact of blur on imagery through a controlled experiment, simulating camera displacement common on UAV flights. The study used the Speeded Up Robust Features (SURF) algorithm for feature detection, which is comparable to SIFT. The study found that blur caused from even a small camera displacement had a large impact on the total amount of image feature points detected in the photos, as well as the amount and correctness of matches found between blurry and sharp images. Consequences of blurry imagery was also reported by Han et al. (2018), who emphasized the negative impact of blurriness in a study of plant-height estimations of Sorghum. Many different factors and circumstances, such as image blur, differing weather conditions, flying patterns and the magnitude of image overlap can therefore affect the end result of the SfM process.

3 Methods

3.1 Study area

The flight imagery used in this study was of maize fields located in the village of Akatawia in the Manya Krobo District in south-eastern Ghana (Fig. 1). The climate in Ghana is largely determined by the seasonal domination of the moist southwesterly winds and the dry northeasterly harmattan winds respectively. Mean annual temperatures are around 26 degrees Celsius and mean annual rainfall is estimated at 1187 mm. Rainfall in the country is unreliable, and the northern parts of the country experience complete crop failures due to low rainfall once in every five years. Annual rainfall can reach 1500 mm per year in the study area and rainfall distribution is bimodal where the larger rainy season occurs between April and early August, while the smaller occurs between September and early November (FAO 2007). In 2016, the growing season was particularly dry in Ghana and a large part of the crops were infested by fall army worm during that year (FAO 2017). Although the specific maize fields modelled in this study were not known to be subject to fall army worm, dry weather conditions might have affected the growth stages of the plants and consequently their geometry in comparison to maize in normal growing conditions. Both maize fields had spot wise incidences of weeds.

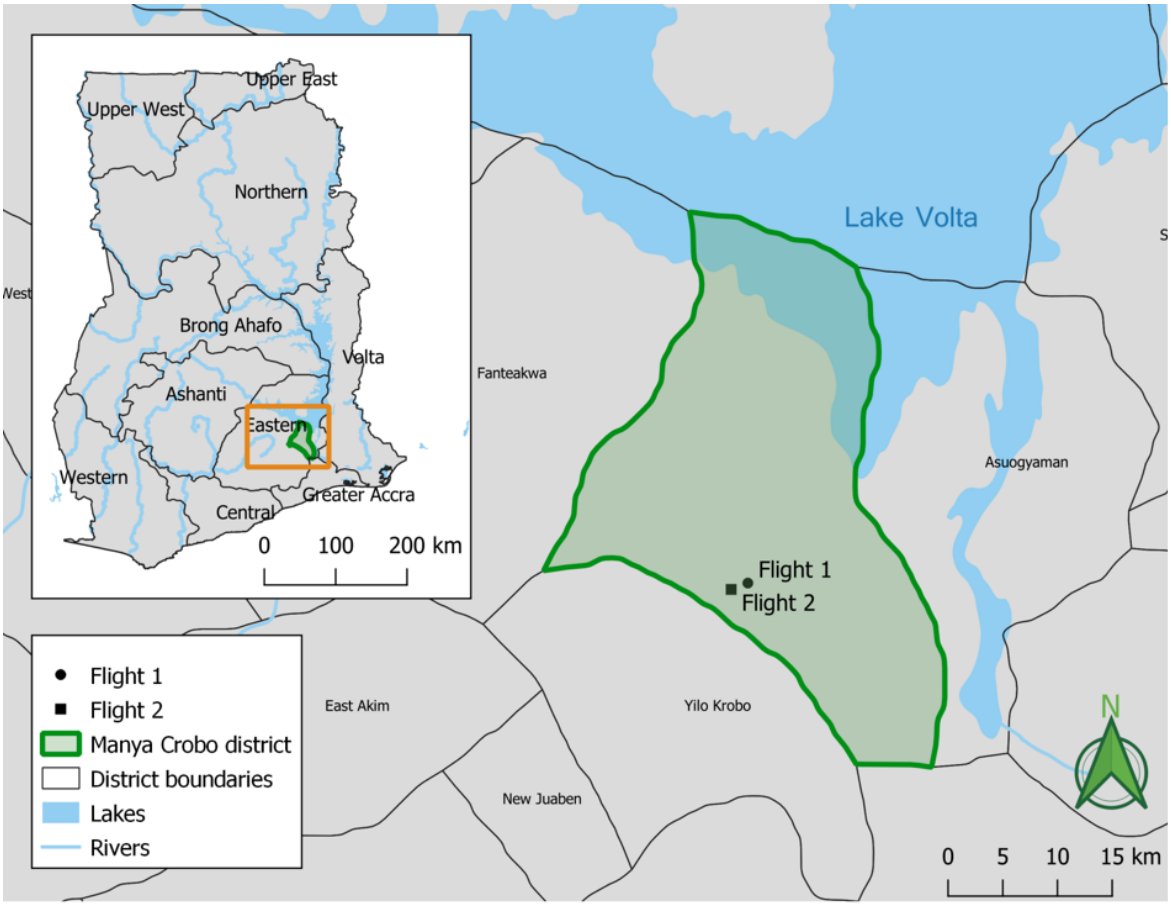

Figure 1. The map shows the location of the two maize fields (Flight1, Flight2) within Manya Crobo district. The smaller map frame (upper left) show the location of the Manya Crobo district within Ghana. Based on data from OpenStreetMap.

3.2 Data and data gathering equipment

The UAV imagery was taken of several maize fields between April and July 2016 during the primary maize growing season. The data was gathered by another group of researchers for the purposes of estimating maize vigor and maize yield using the NDVI. Due to a forward overlap of 80% and a side overlap of 60%, the imagery could also be used to create 3D models by photogrammetric methods as attempted in this study. Two to three flights were done for each maize field, 4-5 weeks after planting (WAP), 8 WAP and 12 WAP. The drone platform was an Enduro Quadcopter from Agribotix (Agribotix 2018) with a Pixhawk flight control system. The RGB imagery was taken by a GoPro Hero 4 camera that was mounted on the drone. The camera was tilted 10 degrees from nadir towards the flight direction, and photos were taken with 1 second intervals on an altitude of 100 m above ground level with a resulting resolution of approximately 3 cm (Wahab et al. 2018). As opposed to De Souza et al.'s (2017) recommendation of using cross directional flights, the flight pattern chosen by the researchers gathering the data was only made in one direction (i.e. NE/SW), possibly because the initial study's intention was not the creation of SfM point clouds.

Flights of two different maize fields are used in this study. Both flights were made after 8-9 WAP when the plants had started their tasseling stage, however the exact planting date might have varied between the two flights. During the tasseling stage, the maize is close to its full height. The flowers, or tassels, developed in this stage might enable the detection of a center point in the maize plant and benefit the explored methods.

Validation data was gathered at one 4 x 4 m subplot in each field by the researchers gathering the data for previously outlined purposes. The field work conducted obtained information of the average maize height, terrain slope, plant density and other measures of the maize in each subplot. Photographs from the subplots of both flights were also taken at the ground at the time of flying (Fig. 3, Fig. 4) (Wahab et al. 2018). Unfortunately, the UAV images were blurry at the location of the subplots in both selected flight cases, meaning the SfM point cloud at those locations might not be reliable. The accuracy of the height estimations of the point clouds as well as the correct amount of maize plants could therefore not be validated from the field data. However, as the subplots are in the vicinity of the areas being analyzed in this study, the field data provided a basis for estimation of the maize height to be used in the data analysis.

From inspecting the UAV images, the light conditions during the flights likely varied and blurry areas were apparent in the images (Fig. 2). Flight 2 had seemingly more variable light conditions between images than Flight 1, and Flight 1 had somewhat less blurry imagery (see appendix A, B and C).

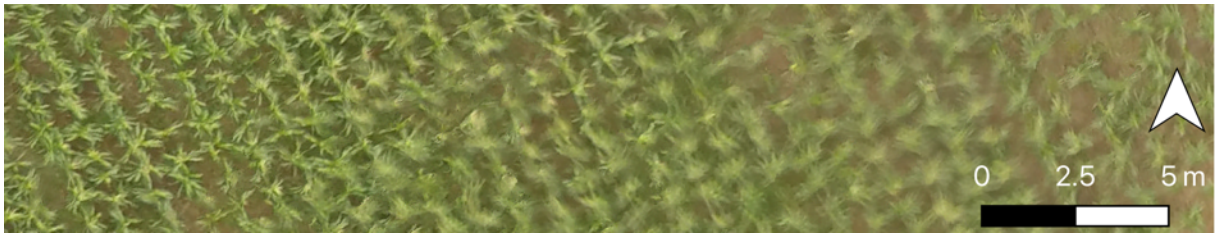

Figure 2. A view of the orthophoto for Flight 2. The incidence of blur can be seen in the mid-right, in comparison to sharper areas on the left.

Figure 3. Maize field of Flight 1, with plants estimated to be approximately 1.7 m tall from field work in subplots. Most of the maize plants have started the tasseling phase.

Figure 4. Maize field of Flight 2, with plants estimated to be approximately 1.8 m tall in the subplots. Most of the maize plants have started to tassel.

3.3 Analysis

3.3.1 Disposition and overview

Two methods were employed in this study and tested on the points clouds created from imagery taken during two different flights. The first method aimed at finding a measure of maize plant density using spatial variations in point heights in a SfM point cloud. The underlying assumption was that an area of dense growing maize will have a canopy that varies less in elevation than an area of sparse growing maize (Fig. 5). The relationship between spatial variation in point heights and maize plant density in an area was tested by using a measure of variance between points in the Z dimension as the independent variable and the number of maize plants as the dependent variable.

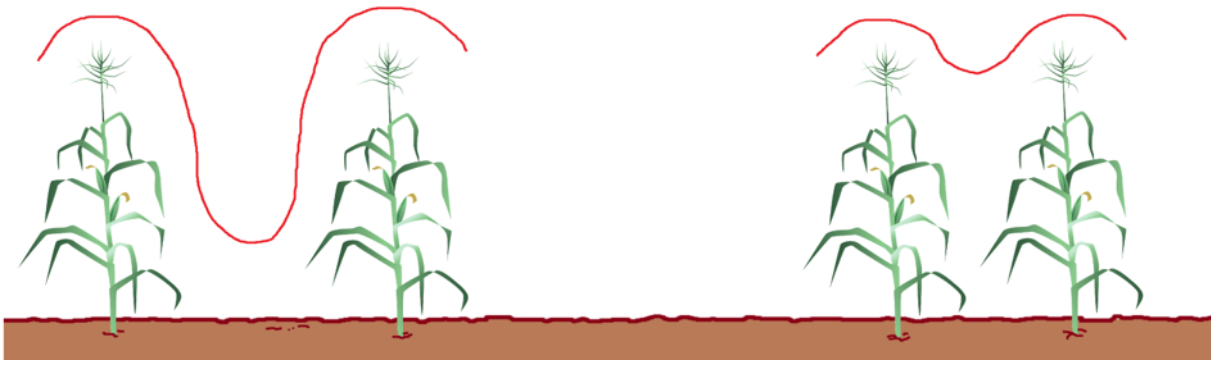

Figure 5. An illustration of the assumption of varying canopy elevation with different maize plant densities in a maize field. Four maize plants are shown, where the two on the left side grow further apart than the two on the right side of the illustration. The red line illustrates potential differences in the magnitude of canopy elevation with differing maize plant density.

The second method attempted to measure maize plant density through distinguishing individual maize plants. This was attempted through creating height contours from a Triangulated Irregular Network (TIN) based on the point cloud, and then querying the resulting contours on elevation and length to extract the ones that represent maize plants.

Before the two methods could be explored, the imagery had to be geotagged, processed into a point cloud and outlying points removed. Different settings used for filtering out outlying points during the dense point cloud creation process were also compared using open source software CloudCompare (CloudCompare 2019). This was to test whether the settings had a significant impact on the resulting point clouds.

3.3.2 Photogrammetric point cloud creation

No ground control points were used for geo-referencing imagery in the study. Instead, the images were geotagged using the open-source ExifTool (Harvey 2019). This software geo-references the imagery by matching the timestamp of the images from the camera clock to the GPS timestamps from the UAV flight logs. The geotagging of imagery likely makes the SfM processing more efficient, and allows the use of a geographic coordinate system throughout the data analysis.

The geotagged images were then imported to PhotoScan (Agisoft LLC 2018) where an automatic image quality estimation was made as a first step to identify photos of low quality. The automatic image quality estimation in PhotoScan finds information on the sharpest border detected in the image, giving an indication of the blurriness of an image (Pasumansky 2014). The photos of the lowest estimated quality were then manually inspected to filter imagery that was deemed inadequate due to being completely blurry. Photos taken at very low altitudes during the start and landing phase of the UAV flight were filtered out. Some higher altitude photos during start and landing, as well as photos taken during the transport stretch to the planned mission starting point were kept. This as they might aid the bundle adjustment step (Frey et al. 2018).

The alignment of the photos was then performed in PhotoScan using the standard upper limits of 40 000 keypoints and 4000 tie points. The concept of keypoints is explained in section 2.4, and the limit determines how many keypoints the software can potentially use to align the imagery. The tie points are those keypoints that have been found in multiple images. The "highest" quality setting was chosen for the photo alignment for maximum accuracy.

Dense point clouds were then generated with the "Ultra high" quality setting, utilizing the full resolution of the imagery on the expense of longer processing time. For the dense point cloud processing, PhotoScan provides the option of choosing between three different depth filtering options: mild, moderate and aggressive. This functionality is aimed at sorting out point outliers and might affect the resulting 3D construction. Point clouds were therefore exported with different settings and compared in CloudCompare using the Cloud-To-Cloud Distance tool to explore possible differences. The tool computes the distance from every point in one point cloud to the nearest neighboring point in the second point cloud. However, a comparison of two point clouds of the same area with different depth filtering settings (mild and aggressive) showed that differences between the point clouds were minimal (Fig. 6), with the mean difference between the point clouds being 0.000312m. The different depth filtering settings were therefore not deemed influential on the analysis, and all point clouds used in this study were consequently created with the "moderate" depth filtering setting.

Lastly, orthomosaics with 3 cm resolution was created for both flights with PhotoScan, based on the image orientation and 3D information generated from the bundle adjustment step (See appendix A, B and C).

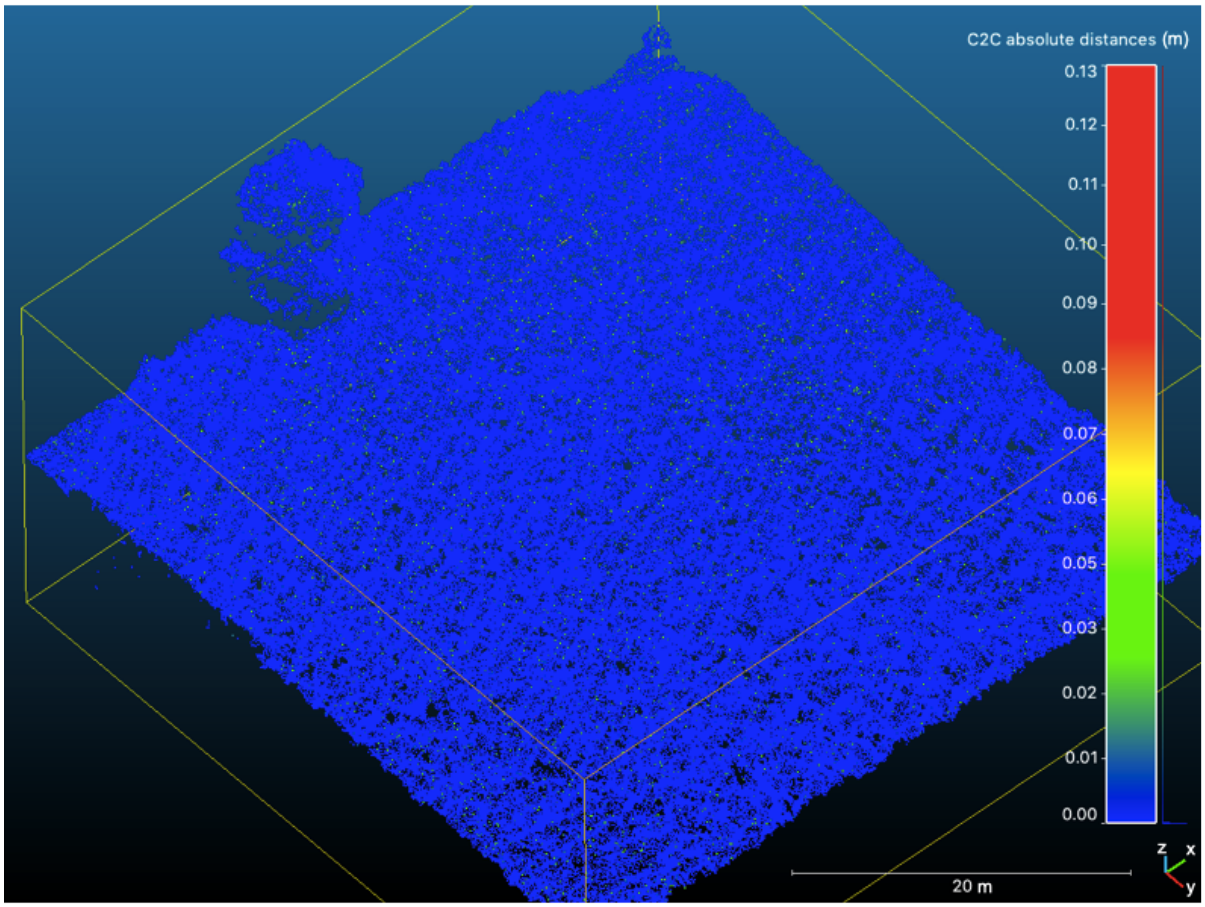

Figure 6. Slightly tilted view from above of the point cloud for Flight 1. The scale denotes the difference in meters between points in the two compared point clouds of different depth filtering settings. Red means large difference and blue means low difference. The differences are seen to be small as few points fall outside the blue spectrum.

3.3.3 Data preparation and point cloud noise removal

The original point clouds from PhotoScan contained a considerable amount of outlying points that needed to be filtered out before analyzing the data. This was done with the partly open-source software LAStools (Isenburg 2019) for the processing of 3D point clouds, as well as with CloudCompare (CloudCompare 2019).

The unlicensed version of LAStools limits the amount of points that can be processed freely, and point clouds containing points above certain limits are automatically slightly distorted. This distortion is in the magnitude of a few millimeters or centimeters but not exactly quantified (Isenburg, M, pers. comm.). Since the data used here were of high resolution and the point cloud was dense, smaller Areas of Interest (AOI) were cut out from the original point clouds to make sure distortions from LAStools were minimized. The AOI's were cut out in areas where the imagery was of highest quality and that contained areas of varying plant densities (Fig. 7).

The AOI point cloud was partitioned in smaller tiles to make processing more efficient. Outlier points were then identified with a LAStools algorithm that uses a 3D grid of cells of a predefined size and a defined maximum number of points. If the number of points within the cell is below the defined maximum, the points are classified as noise. A cell size of 0.8 x 0.8

by 0.5 m was defined, with a maximum of 200 points. These settings identified the most obvious outliers while infringing minimally on points that were correctly placed. Lastly, the tiles were merged, while excluding points classified as noise.

Five training and two validation areas of 4 x 4 m were then chosen within the AOI for each of the two flights, totaling 14 sample areas for both flights combined. These were purposefully sampled using the orthomosaics of the respective flights. Attempts were made to ensure different maize densities within the five training areas (T1-T5), and to create validation areas of both sparsely growing maize (SVA) and dense growing maize (DVA). The number of samples was to some extent limited due to the occurrence of blur in the orthomosaics (Fig. 7). The sample area size of 4 x 4 m was chosen with the intention of including a large enough area to sample a representative plant density while still capturing local variations. The sample areas were aligned along the maize rows in order to ensure as few partly cut off maize plants as possible. The sample areas for Flight 2 can be seen in Appendix D.

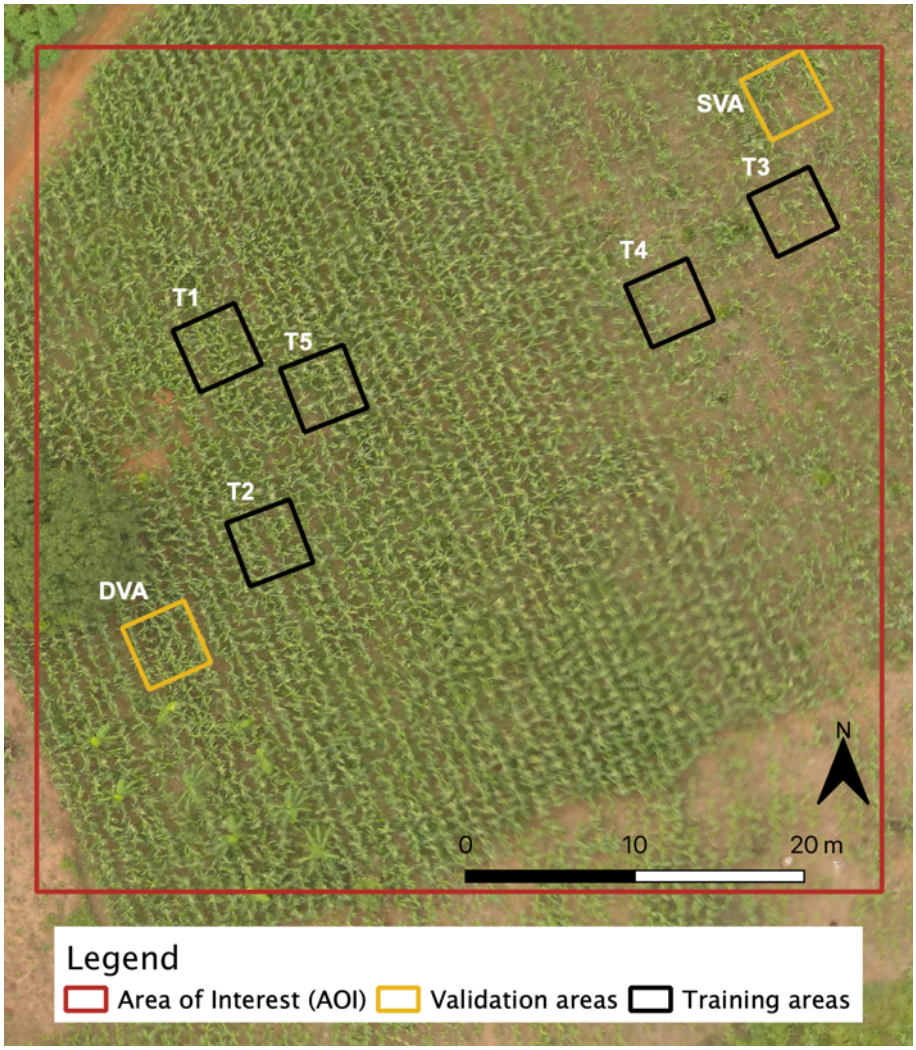

Figure 7. The area of interest (AOI) of Flight 1 (red rectangle), containing five training areas ($T1_1$-$T5_1$) (black squares) and the dense (DVA_1) and sparse (SVA_1) validation areas (yellow squares) of varying maize plant densities.

The sample areas were then clipped out from the AOI point clouds, resulting in seven point clouds for each flight. According to the previously conducted field survey (Wahab et al. 2018), the height of the maize was approximately 1.7 to 1.8 m high in the chosen maize fields. However, the elevation span between the highest and the lowest located point in the point clouds of the areas were considerably larger than that, meaning outliers likely remained in the point clouds. In addition to the initial noise removal using LAStools, a statistical outlier removal (SOR) filter was therefore applied to all the areas using CloudCompare. This filter computes the average distance from one point to K nearest neighbors, and removes points at a distance larger than the average distance plus N times the standard deviation of the point cloud. In this case, K and N were set to 6 and 4 respectively, as these settings removed outliers without generally thinning out the point clouds.

An elevation threshold (Z threshold) of 2 m below the highest located point was then defined for all training and validation areas and all points below this threshold were removed to increase the likelihood that remaining points were located between the maize plant canopy and the ground level.

An overview of the described point cloud creation process as well as the removal of outlying points can be seen in figure 8.

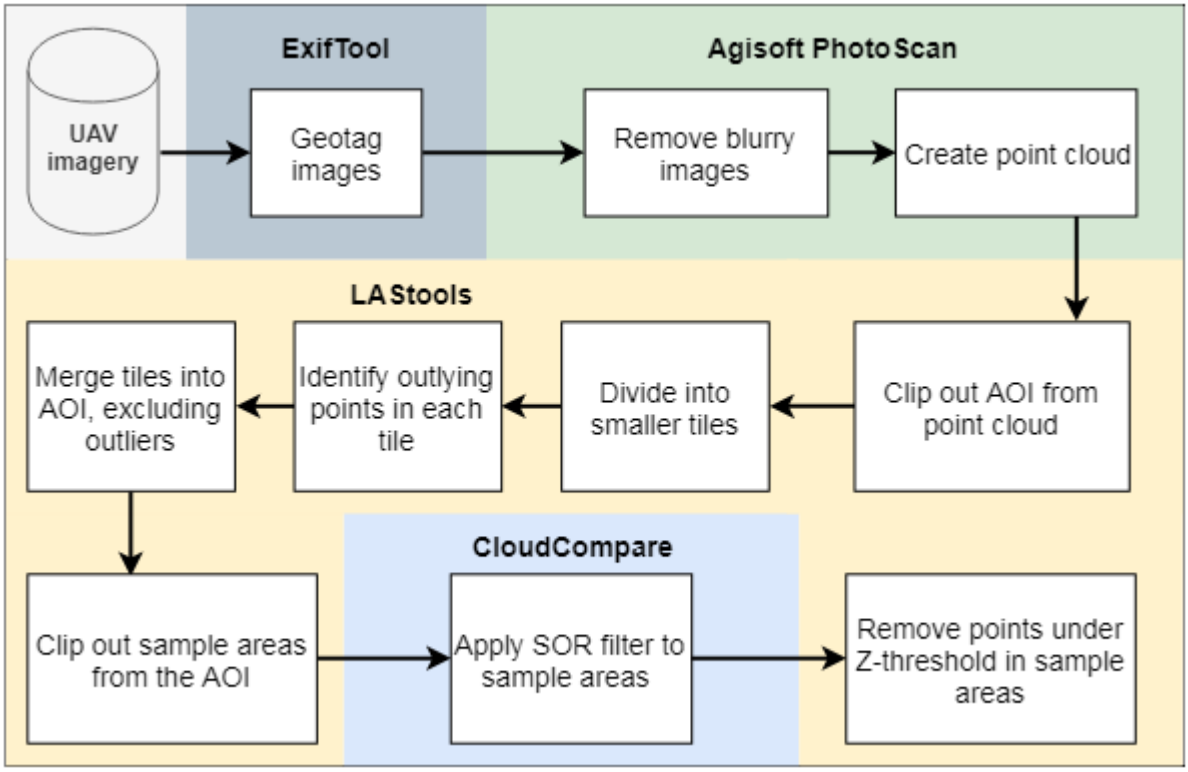

Figure 8. The workflow from UAV imagery to fully processed sample areas, with colors corresponding to different softwares used for the processing steps. Images were geotagged with ExifTool and then imported to PhotoScan to be processed into a point cloud. Areas of Interest (AOI) were clipped out from the point cloud. Outliers were removed from the AOIs and sample areas were clipped out using LAStools. A statistical outlier removal (SOR) filter was applied in CloudCompare to all sample areas. Finally, all points below a certain elevation (Z-threshold) were removed in each sample area.

The number of individual maize plants were lastly visually estimated within the training and validation areas using the orthomosaics of the respective flights (Fig. 9). Since the maize plants number and location could not be validated on the ground, the estimated and true maize plant count as well as their location can differ.

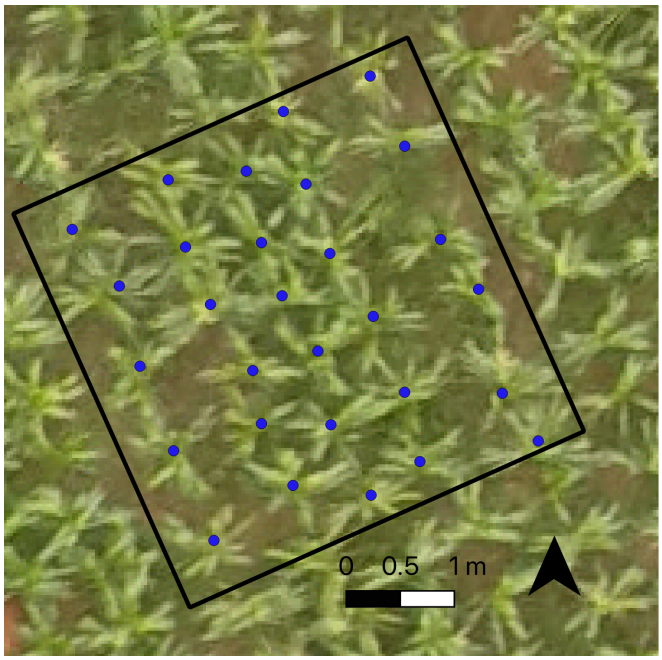

Figure 9. The maize plants were counted visually in each sample area (black square) from inspecting the orthomosaics of the UAV imagery. The blue points in the image show the location of the counted maize plants.

3.4 Method 1: Detecting maize plant density from canopy structure

In method 1, a simple linear regression was used to explore a potential relationship between standard deviation of point height in the point cloud and the estimated number of maize plants in an area. The regression equation was then used to predict maize plants in an area using the average standard deviation (SD_{avg}) of point heights in that area. An overview of the complete workflow for method 1 can be seen in figure 11.

Firstly, raster grids were created based on the point clouds of each sample area, where each cell in the grids corresponded to the standard deviation of point heights at that location (Fig. 10). This step was completed using LAStools. To ensure that the underlying point sample for each cell was sufficient to constitute a measure of standard deviation, only cells where the centroid fell inside the sample area was kept. To explore the relation between standard deviation and cell size, 20 grids with different cell sizes were created for each area. These cell sizes ranged between 0.05 m and 1 m with 0.05 m intervals. The SD_{avg} was then calculated for every grid in every sample area, to derive a measure of point height variations per area.

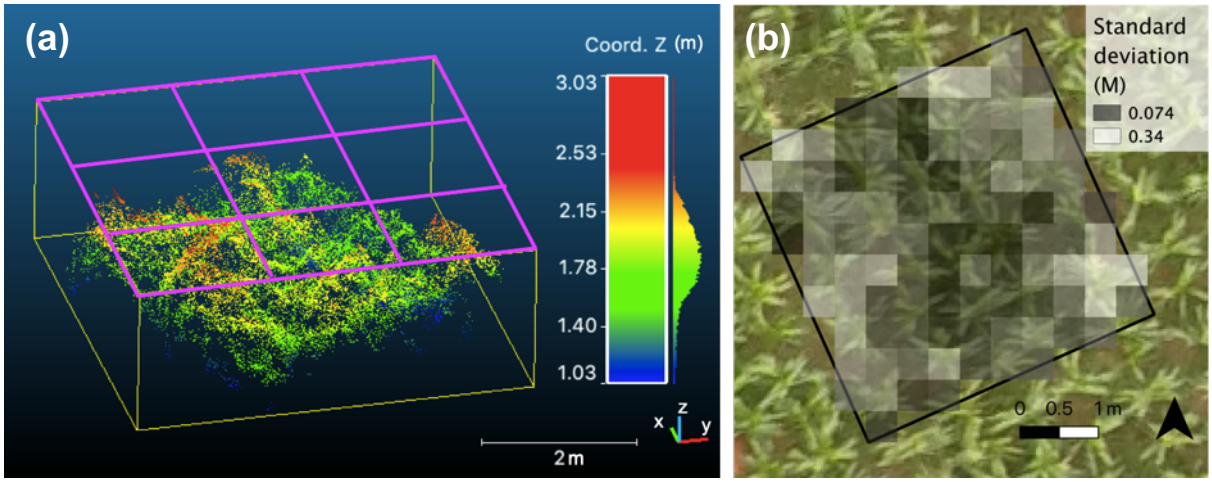

Figure 10. (a) shows a point cloud from a sample area with a fictitious 3 x 3 cell grid above it (pink grid). All cells in the grid have values from calculating the standard deviation of elevation variations of the points directly below each cell. (b) shows an example of a real grid with standard deviation values within a sample area. The grid has cell sizes of 0.4 x 0.4 m and is one of 20 grids with different cell sizes that were calculated for each sample area.

To explore the impact of cell size on the average standard deviations in the sample areas, the SD_{avg} for each grid of different cell size was plotted for all areas.

The number of maize plants and the SD_{avg} calculated from the grids with differing cell sizes were then plotted against each other to visualize a potential relationship. Regressions were then calculated between the number of plants and SD_{avg} derived using different cell sizes in each sample area (Eq.1).

$$N = SD_{avg} * K + I \qquad \textit{(Eq. 1)}$$

Where K is the slope of the line, I is the intercept, N is the number of maize plants and SD_{avg} is the average standard deviation of the sample area.

Since every area had 20 different SD_{avg} values calculated using different cell sizes, this resulted in 20 regression equations per area. Furthermore, the 20 regressions were calculated using the training areas of Flight 1 and 2 separately, as well as with the training areas from both flights combined. These are presented in three separate sections in the result. The reason for this was to test for the influence of differing point cloud quality, maize heights and spatial distribution of plants between the flights.

The coefficient of determination (R^2) as well as probability-values were used to test the strength and significance of a potential linear relationship between the two variables. A significance level of 0.05 was set. R^2 and probability-values were calculated for all 20 regressions of each flight to answer RQ2 regarding whether an optimal sampling cell size of the standard deviation grids could be found.

In order to predict the number of maize plants, the SD_{avg} for the validation areas in all resolutions was then input to the equations as the independent variable. This resulted in an estimated plant density per validation area for each resolution. The reason for this was to see how well the model would predict the maize plant density in relation to the plant count in the validation areas.

Lastly, the model was used to predict maize plant density on a field scale. The AOI of Flight 1 was chosen for this analysis due to its estimated lower blurriness and more even light conditions during flight. At first, a grid of 4 x 4 m cells was created from the AOI, where every cell corresponded to the standard deviation of point heights at that location. A regression equation of high R^2 values was then used to predict the maize plant density in every cell, by using the standard deviation values as the independent variable. The results were compared visually to the orthomosaic of the same area, to answer RQ1 of whether the method could give an indication on plant densities within a maize field.

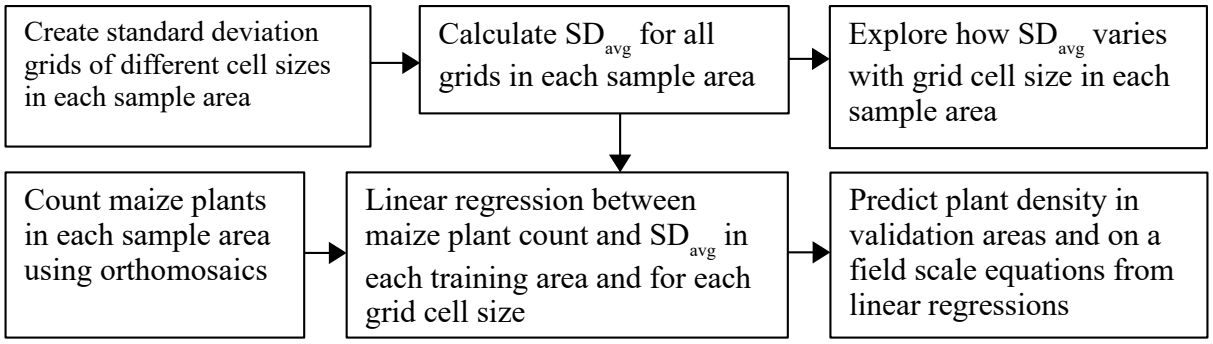

Figure 11. Workflow for method 1. Raster grids of different cell sizes were first calculated in each sample area. Cell values in these grids corresponded to the standard deviation of the points heights in the sample areas. The average standard deviation (SD_{avg}) was then calculated for all grids in each sample area. A regression was then made between the estimated plant count, and the SD_{avg} for every grid in each of the training areas. The resulting equations were then used for predicting the maize density in the validation areas. Lastly, a regression equation was chosen based on the R^2 values of the different regressions to predict maize plant density on a field scale.

3.5 Method 2: Detecting maize plants from elevation contours

The second method attempted to estimate maize density through delineating individual maize plants from a Triangular Irregular Network (TIN). This was done through creating a continuous surface through triangulation of the point cloud, and then generating elevation contours based on this surface (Fig. 12).

Elevation contours based of the point clouds of the dense and sparse validation areas in each flight were created using the 'las2iso' tool in LAStools. This tool triangulates the point cloud to create a temporary TIN, on which it bases the creation of contour lines. In the parameters for the tool, the intervals between elevation contours can be set. In this case, elevation contours with 0.05, 0.1, 0.15 and 0.2 m intervals were tested to see which elevation interval best captured the maize plants with the least amount of noise. The resulting contours were then queried on Z values of approximately 1 m below the highest located point in all areas, and with restrictions on both minimum and maximum length of contours. The querying on height was done in an attempt to exclude points in the point clouds that did not correspond to maize plants. The querying on contour length was done in an attempt to exclude very small and scattered contours as well as long contours outlining larger areas.

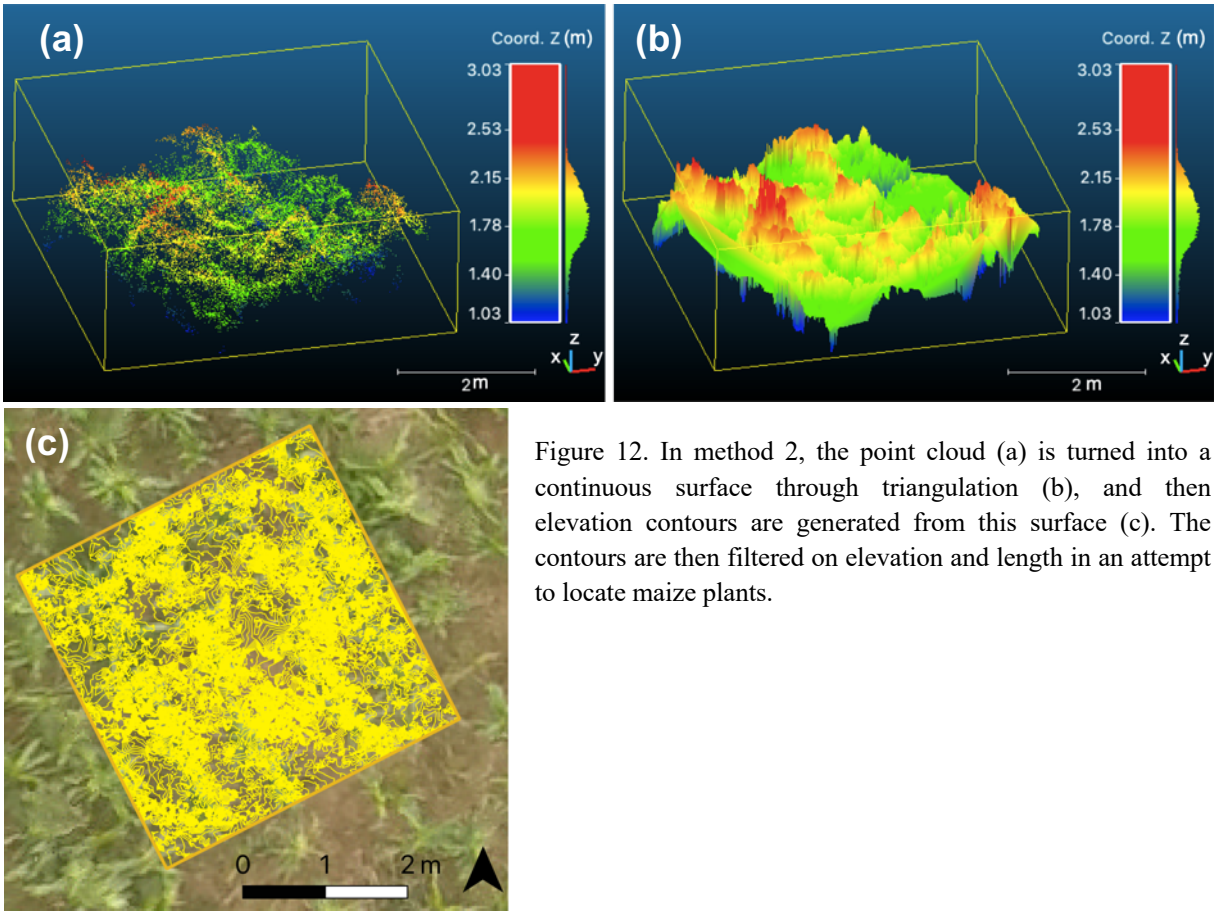

Figure 12. In method 2, the point cloud (a) is turned into a continuous surface through triangulation (b), and then elevation contours are generated from this surface (c). The contours are then filtered on elevation and length in an attempt to locate maize plants.

4 Results

4.1 Point cloud exploration

Views of the point clouds for Flight 1 and Flight 2 can be seen in figure 13, with points having RGB values from the UAV imagery. Upon visual inspection, both point clouds have an appearance resembling a maize field, with visibly clear maize rows as well as surface variations in every row that resembles maize plants. The red lines in the respective image show the location of transect lines of the point clouds created to inspect the elevation profile along a maize plant row (Fig. 14 and 15).

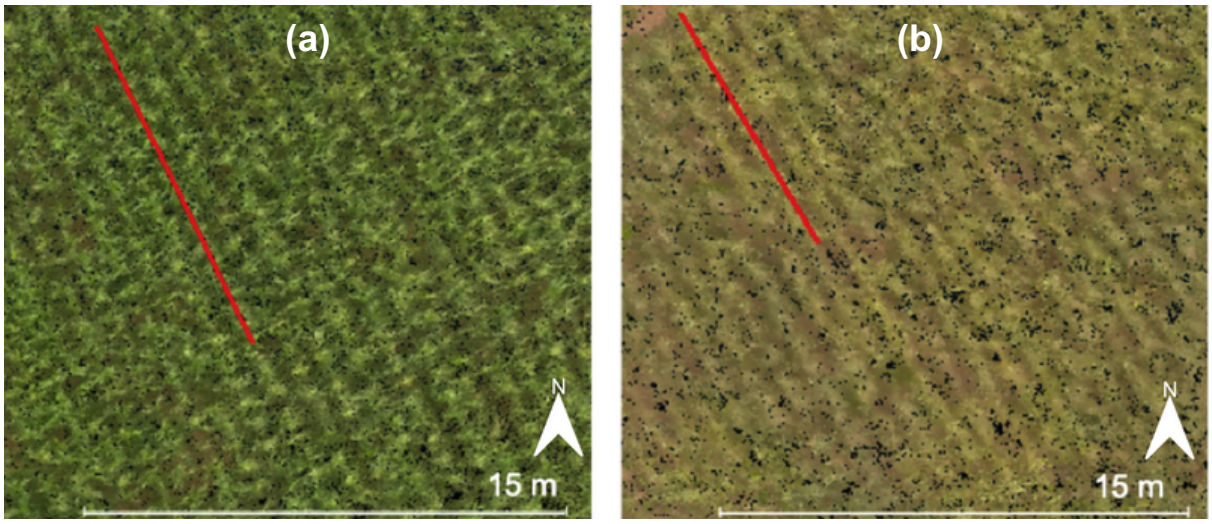

Figure 13. (a) shows a view of the point cloud for Flight 1 and (b) shows the point cloud for Flight 2. Clear rows are visible in both flights, as well as height differences within the rows representing the different maize plants. The red line in respective image shows the location of elevation transects along a maize plant row (Fig. 14 and 15).

Point cloud transects are seen for Flight 1 (Fig. 14) and Flight 2 (Fig. 15), and show the differences in point-elevation along a row of maize plants. Peaks and valleys along the transect indicate the presence of individual plants.

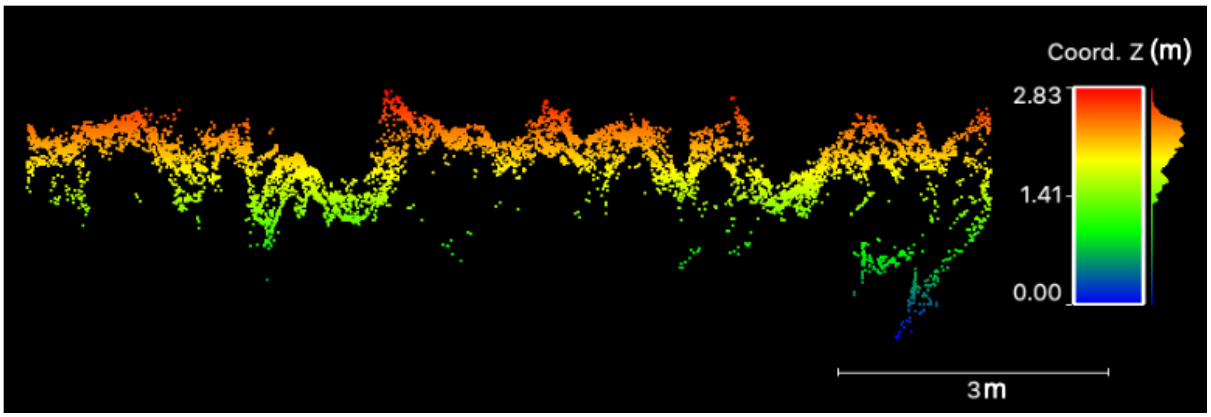

Figure 14. A transect profile of a point cloud for Flight 1 along a maize row. The coloring of points indicates their altitude. Peaks and valleys in point altitude are visible, likely indicating positions of individual plants.

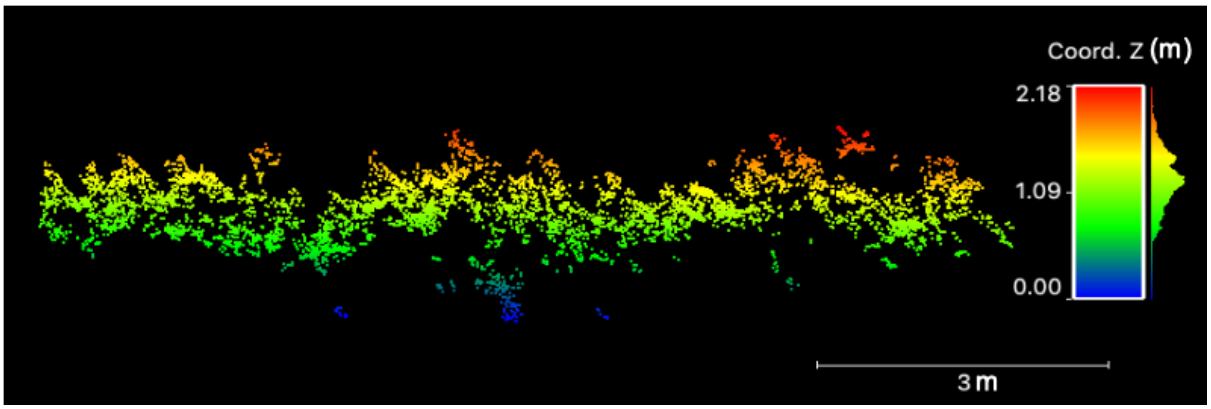

Figure 15. A transect profile of a point cloud for Flight 2 along a maize row. The coloring of points indicates their altitude. Peaks and valleys in point altitude are visible, likely indicating positions of individual plants.

Information about all training and validation areas, including the number of estimated plants in the area (Plant count), the initial elevation span before applying the Z threshold between the highest and the lowest located point (Orig. Z span) as well as the total number of points in respective sample area (Point count) are seen for Flight 1 (Table 1) and Flight 2 (Table 2). For Flight 1, the original Z span varied approximately 0.7 m between the area with the highest ($T5_1$) and the lowest Z span (SVA_1). The DVA_1 had the highest point count while the SVA_1 had the lowest point count.

For Flight 2, the original Z span varied approximately 1.39 m between the area with the highest ($T3_2$) and the lowest ($T5_2$) Z span. $T5_2$ had the lowest and $T3_2$ the highest point count.

Table 1. Information about all the training ($T1_1$-$T5_1$) and validation areas for Flight 1, including the number of plants counted per area, the total number of points and the original span between the highest and lowest located point before applying the 2 m height threshold.

	$T1_1$	**$T2_1$**	**$T3_1$**	**$T4_1$**	**$T5_1$**	**DVA_1**	**SVA_1**
Plant count	29	24	18	18	22	30	23
Orig. Z span (m)	3.02	2.64	2.44	3.09	3.21	2.56	2.38
Point count	26740	26214	21387	22952	27577	29607	18741

Table 2. Information about all the training ($T1_2$-$T5_2$) and validation areas for Flight 2, including the number of plants counted per area, the total number of points and the original span between the highest and lowest located point before applying the 2 m height threshold.

	$T1_2$	**$T2_2$**	**$T3_2$**	**$T4_2$**	**$T5_2$**	**DVA_2**	**SVA_2**
Plant count	22	19	22	13	24	21	17
Orig. Z span (m)	3.42	3.68	3.83	2.49	2.44	3.27	3.00
Point count	18030	17979	22580	19798	17853	21379	21054

4.1.1 Point cloud histograms of sample areas

4.1.1.1 Sample areas of Flight 1

The point frequency (Y axis) per elevation value (X axis) for the DVA_1, SVA_1 and T_1 - T_5 are shown in figure 16. Elevation values in the histograms are expressed in a local coordinate system used by CloudCompare; however, the X-axis value range is approximately 2m for all areas. Sparser areas such as $T3_1$, $T4_1$ and the SVA_1 show a broader distribution over the range of elevations while the denser $T1_1$ and $T2_1$ areas displays a more concentrated point distribution. The DVA_1 has a high concentration of points on higher elevations but also shows a slightly elevated tail in lower elevations. A long right-hand tail with a low point frequency can be noticed for $T1_1$, $T4_1$ and $T5_1$.

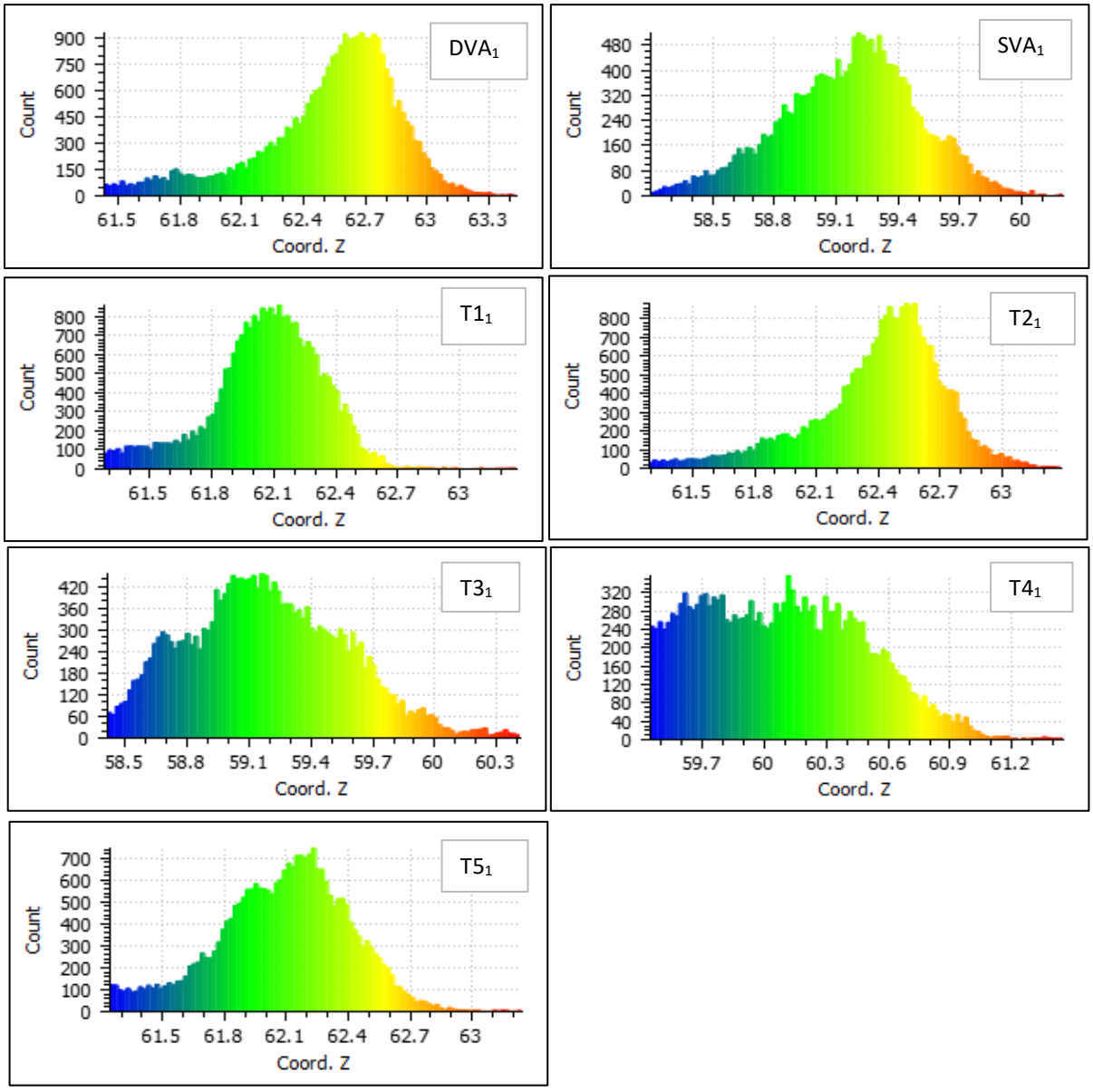

Figure 16. The figure shows histograms of point count (Y-axis) per elevation (X-axis) for the DVA_1, SVA_1 and T_1 to T_5.

4.1.1.2 Sample areas of Flight 2

The point frequency (Y axis) per elevation value (X axis) for DVA_2, SVA_2 and $T1_2$ - $T5_2$ are shown in figure 17. The sparser areas such as the SVA_2, $T2_2$ and $T4_2$ have a broader point distribution over the range of elevations while the denser $T5_2$, $T3_2$ and $T1_2$ areas displays a slightly more concentrated distribution. The DVA_2 in contrast also displays a relatively broad point distribution. The $T1_2$, $T3_2$ and DVA_2 have long right-hand tails with low point frequencies.

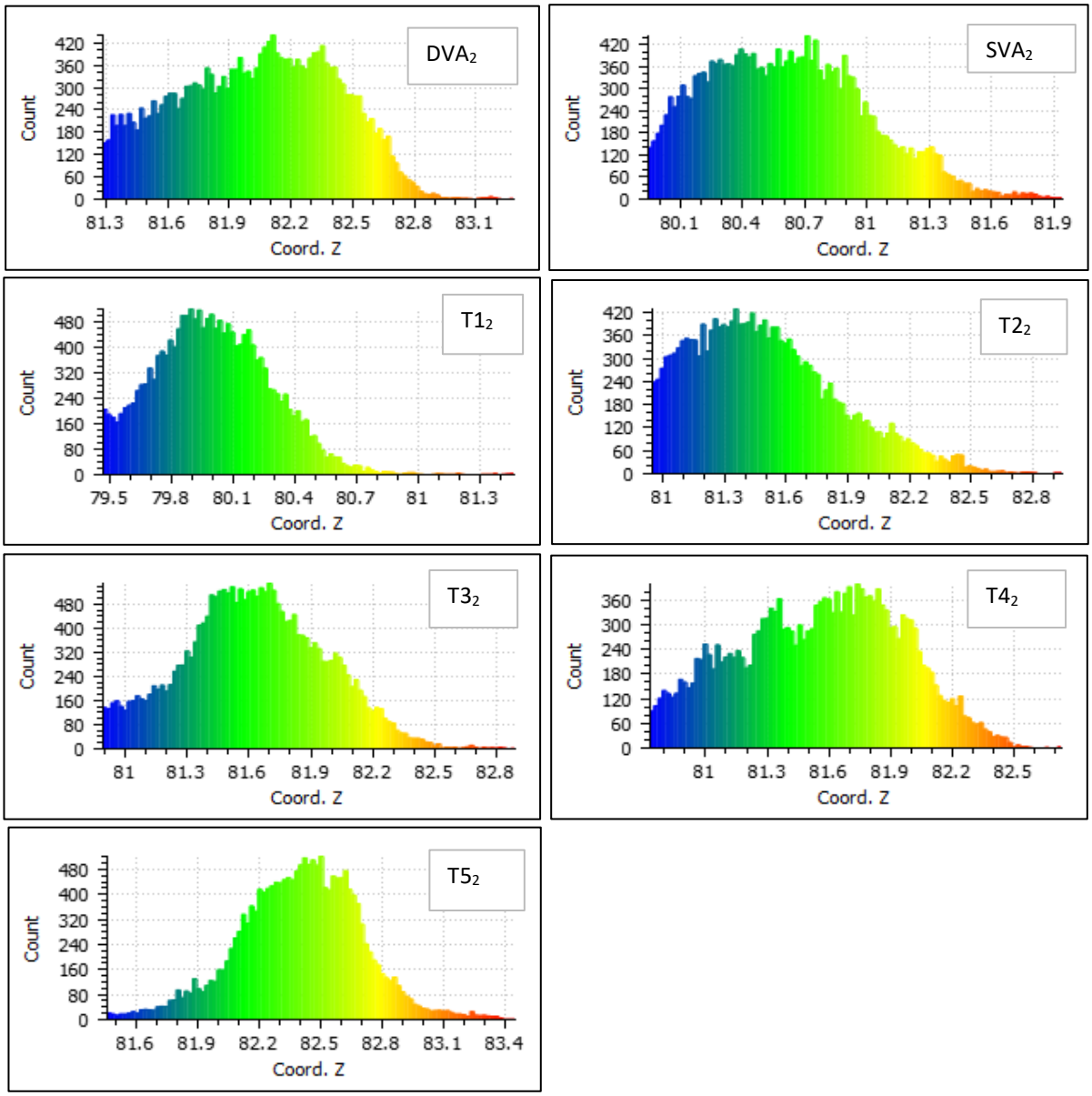

Figure 17. The figure shows histograms of point count (Y-axis) per elevation (X-axis) for the DVA_2, SVA_2 and $T1_2 – T5_2$.

4.2 Method 1: Detecting maize plant density from canopy structure

4.2.1 Flight 1

4.2.1.1 Average standard deviation plotted against cell size

The SD_{avg} calculated using different cell sizes is plotted for all training and validation areas in Flight 1 (Fig. 18). There is a trend of increasing SD_{avg} with larger cell sizes. The SD_{avg} also fluctuates more with larger cell sizes, from approximately 0.55 m and larger cell sizes. All areas except the DVA_1 exhibit a lower SD_{avg} with a higher number of maize plants, with $T3_1$ (18 maize plants) showing the highest SD_{avg} using most cell sizes. The DVA_1 deviates as it has the highest number of plants (30 plants) and still among the highest SD_{avg} across the different cell sizes.

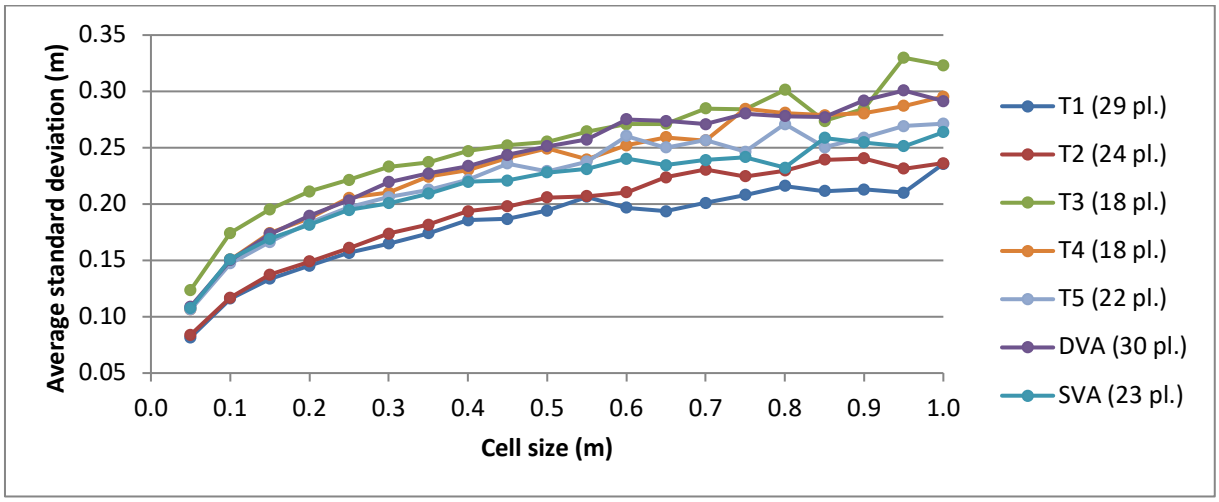

Figure 18. The graph shows average standard deviation of the training areas ($T1_1$-$T5_1$) and the dense and sparse maize validation areas plotted against all cell sizes. The number of maize plants in each area is noted in the parenthesis in the legend on the right.

4.2.1.2 Linear regressions between number of plants and average standard deviation

Linear regressions between SD_{avg} and the number of maize plants in the training areas was calculated using all cell sizes. Regressions for the 0.2, 0.5 and 0.8 m cell sizes are plotted in figure 19. The circles represent the five training areas while triangles correspond to the DVA_1 and the SVA_1. The trend lines indicate a negative relationship between the number of plants and the SD_{avg}. The SVA_1 aligns well will the trend, while the DVA_1 strongly deviates from the model. The goodness-of-fit differed for regressions using different cell sizes for calculating SD_{avg} (Fig. 20), where the regression with 0.85 m cells showed the best goodness-of-fit ($R^2 = 0.99$) and the regression with 0.55 m cells the lowest goodness-of-fit ($R^2 = 0.74$).

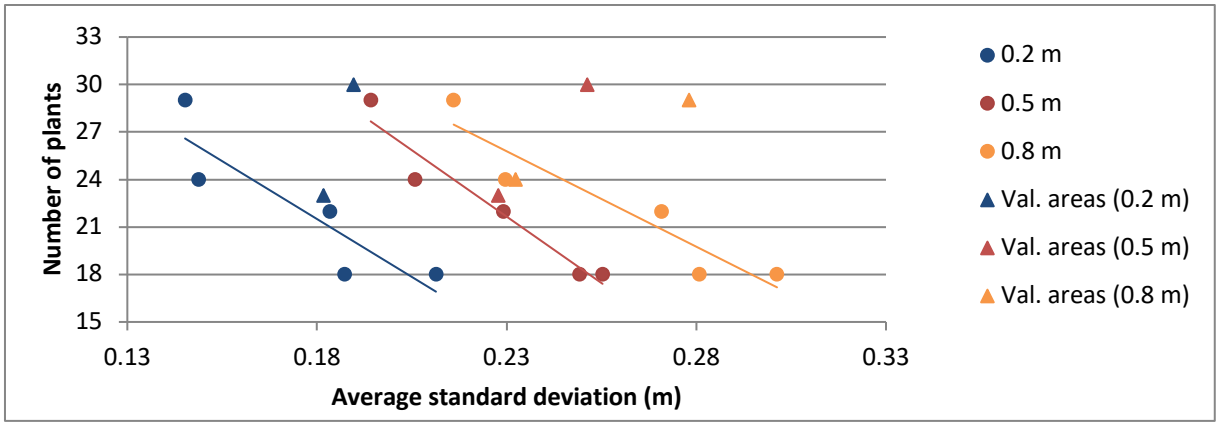

Figure 19. The average standard deviation (SD_{avg}) of the training areas is plotted against the estimated number of maize plants for cell sizes of 0.2, 0.5 and 0.8 m (circles). A negative relationship between the number of plants and the SD_{avg} of the training areas is indicated by the trend lines. The number of plants and SD_{avg} of the dense and sparse validation areas (triangles) are plotted as reference.

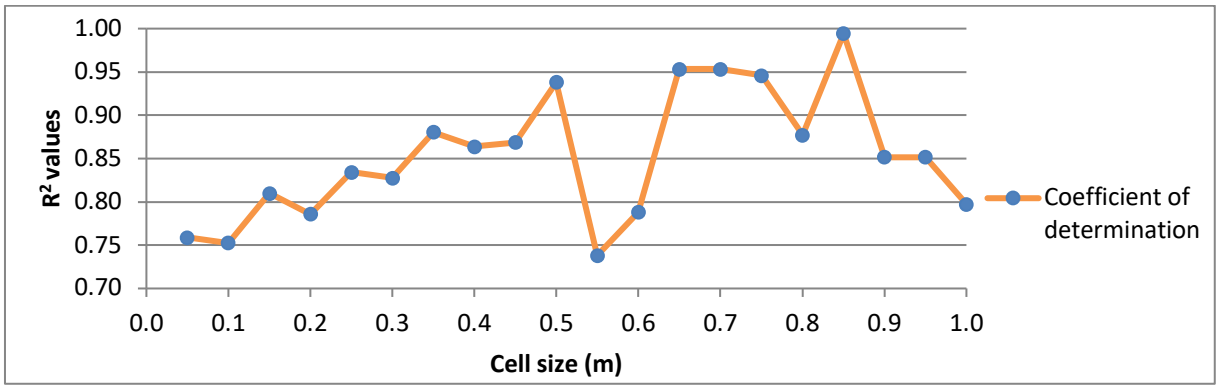

Figure 20. Blue circles represent the R^2 values of regressions between average standard deviation and the maize plant count. Regressions were calculated with different cell sizes and all are presented in the graph. R^2 values initially increase with cell size, and varies more with larger cell sizes.

4.2.1.3 Prediction of dense growing maize

Figure 21 shows predictions of maize plant count from the linear regressions for the DVA_1. The predictions vary slightly with cell size used for the regression and are consistently lower than the estimated number of plants in the validation area.

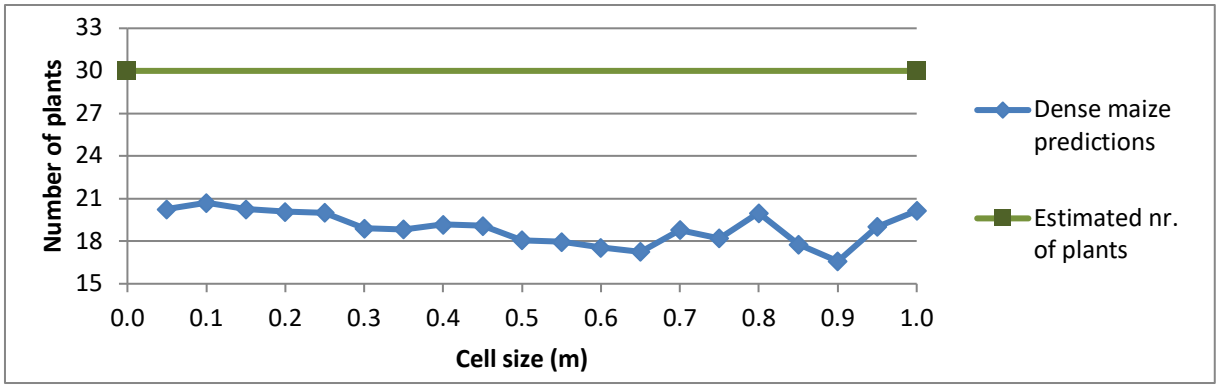

Figure 21. Predictions of the number of maize plants in the validation area of dense growing maize of Flight 1. Predictions are derived from the regressions between SD_{avg} and maize plant count calculated using different cell sizes.

4.2.1.4 Prediction of sparse growing maize

Figure 22 shows predictions of maize plant count from the linear regressions for the SVA_1. The predictions vary with cell size used for the regression, and a trend of higher predictions can be seen with larger cell sizes. The predictions are within three plants of the estimated plant count (23 plants), with regressions using 0.65 – 0.75 m and 1.0 m cell sizes giving the most accurate predictions.

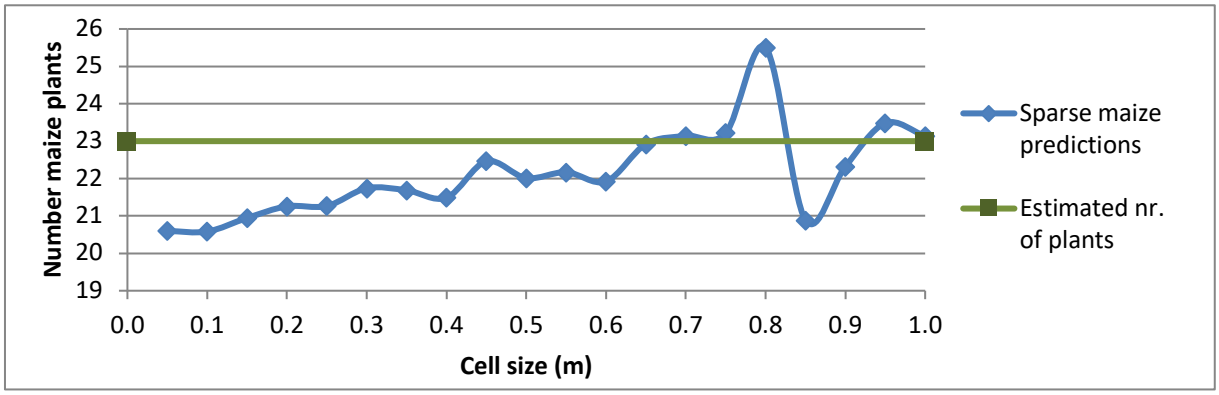

Figure 22. Predictions of the number of maize plants in an area of sparsely growing maize. Predictions are derived from the regressions between SD_{avg} and maize plant count calculated using different cell sizes.

4.2.2 Flight 2

4.2.2.1 Average standard deviation plotted against cell size

The SD_{avg} calculated using different cell sizes is plotted for all training and validation areas in flight 2 (Fig. 23). There is a trend of increasing SD_{avg} with larger cell sizes for all areas. SD_{avg} also fluctuates more with larger cell sizes, from approximately 0.8 m onwards. $T2_2$ and the SVA_2 have low maize plant densities and display relatively high SD_{avg}. $T1_2$ and $T4_2$ have relatively high maize plant densities and display lower SD_{avg}. In contrast to this, the DVA_2 (21 plants) has the highest SD_{avg} across the areas, while $T4_2$ (13 plants) has among the lowest SD_{avg}.

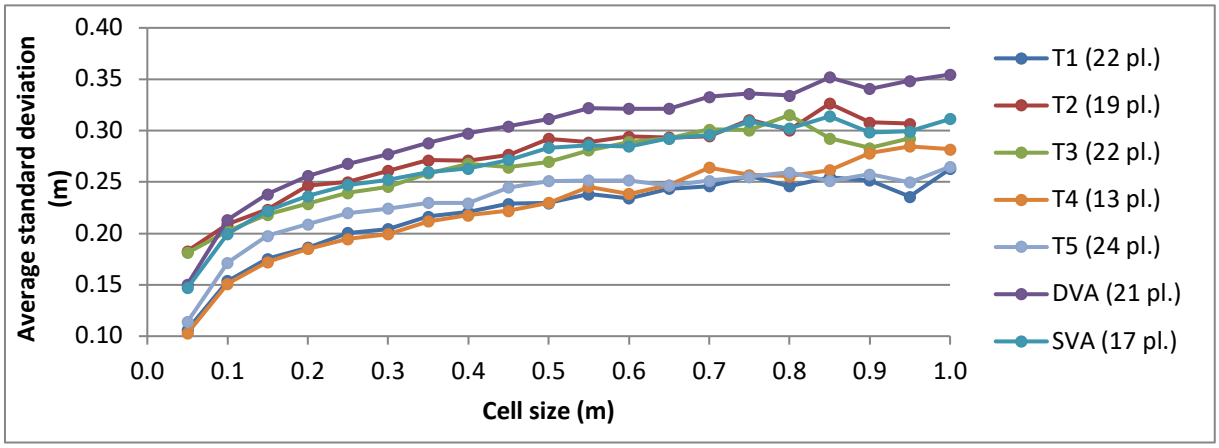

Figure 23. Average standard deviation plotted for all areas and cell sizes (m) in Flight 2. The number of maize plants in each area is noted in parenthesis in the legend on the right.

4.2.2.2 Linear regressions between number of plants and average standard deviation

Linear regressions between SD_{avg} and the number of maize plants in the training areas was calculated using all cell sizes. Regressions for the 0.2, 0.5 and 0.8 m cell sizes are plotted in figure 25 and the trend lines indicate a negative relationship between the two variables. $T4_2$ was omitted from the regressions, as it was deemed an outlying sample area. This is further explored in section 4.2.4 (Fig. 35). The circles in the graph represent the four remaining training areas while triangles correspond to the DVA_2 and the SVA_2. The coefficient of determination differs between regressions calculated using different cell sizes (Fig. 26), with the regression using 0.9 m cell sizes displaying the highest goodness-of-fit ($R^2 = 0.72$).

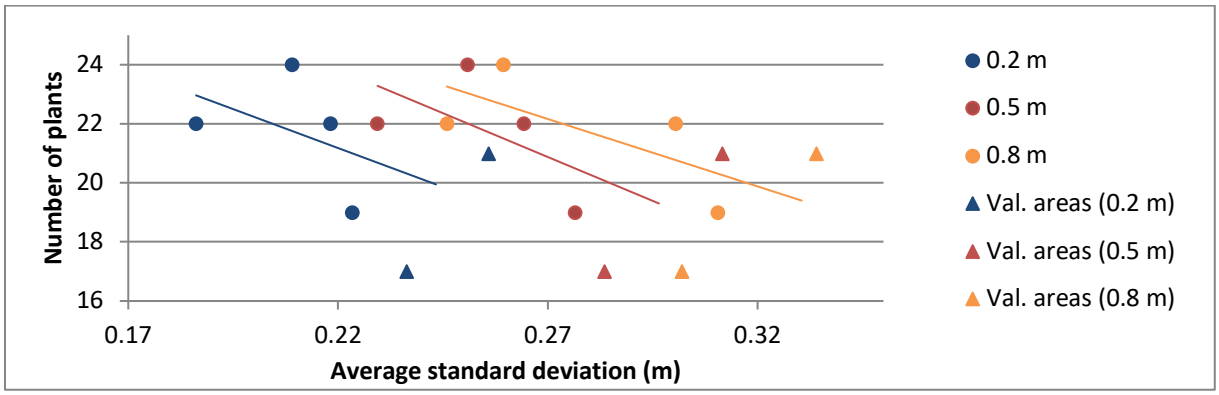

Figure 25. The average standard deviation (SD_{avg}) of the training areas (circles) are plotted against the estimated number of maize plants for the resolutions 0.2, 0.5 and 0.8 m. A negative relationship between the number of plants and the SD_{avg} of the training areas is indicated by the trend lines. The number of plants and SD_{avg} of the dense and sparse validation areas (triangles) are plotted as reference.

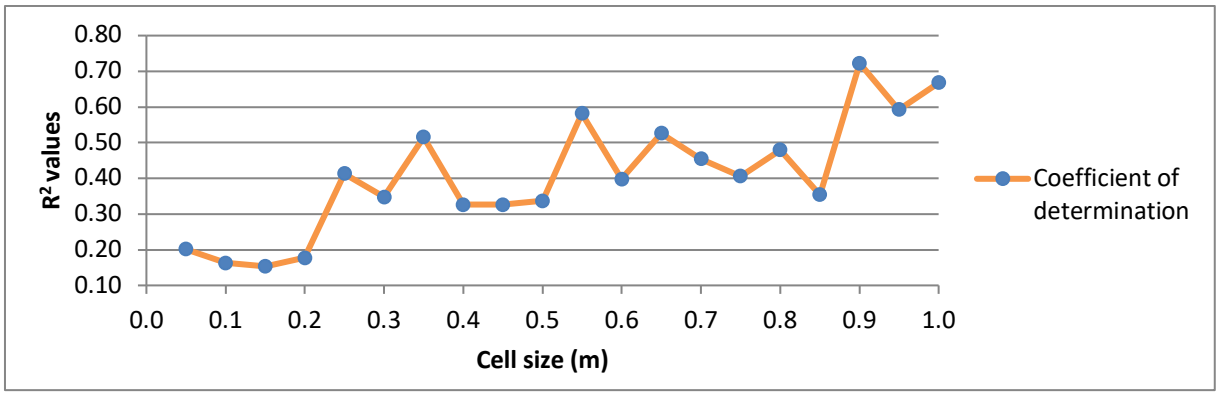

Figure 26. The blue circles represent the R^2 values of regressions between average standard deviation and the maize plant count. The regressions were calculated using different cell sizes and all are presented here. The R^2 values are low for the smallest cell sizes and a general trend of increased R^2 values with cell size can be seen, although variations are large.

4.2.2.3 Prediction of dense growing maize

Figure 27 shows predictions of maize plant count from the linear regressions for the DVA_2. The predictions are consistently lower than the estimated number of plants in the validation area, and vary between approximately 19 and 16 maize plants. A trend of lower predictions for regressions using the largest cell sizes can be seen.

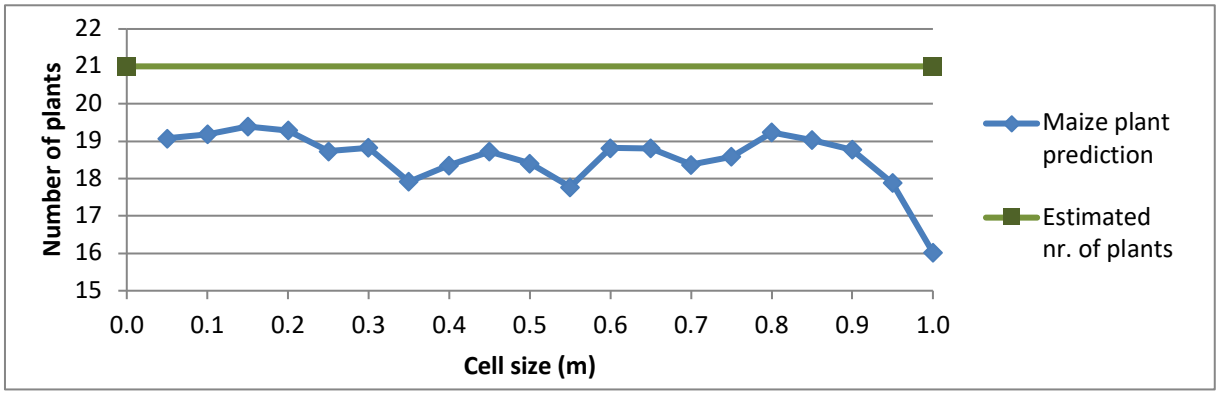

Figure 27. The graph shows the different predictions of the number of maize plants in a validation area of dense growing maize. Predictions are derived from the regressions between SD_{avg} and maize plant count calculated using different cell sizes.

4.2.2.4 Prediction of sparse growing maize

Figure 28 shows predictions of maize plant count from the linear regressions for the SVA_2. The predictions are consistently higher than the estimated number of plants in the validation area, and vary between approximately 19 and 21 maize plants.

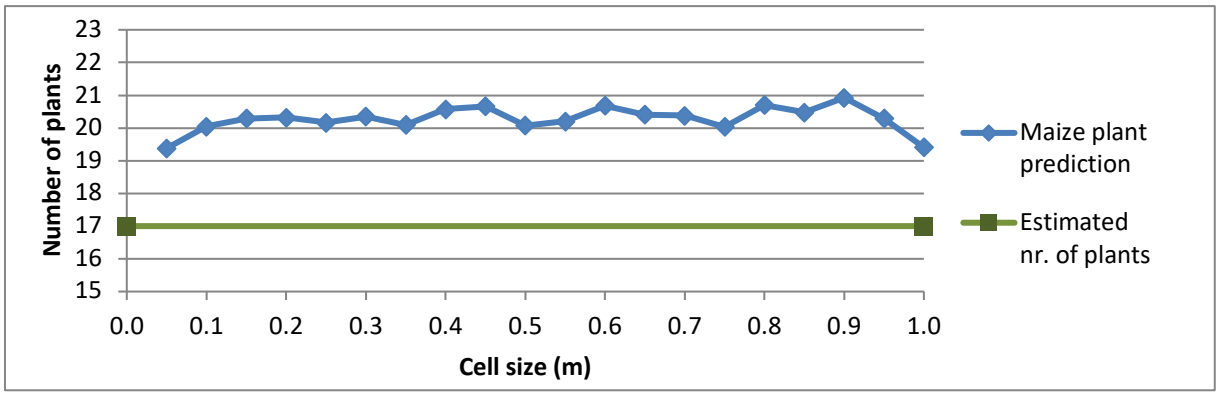

Figure 28. The graph shows the different predictions of the number of maize plants in a validation area of sparse growing maize. Predictions are derived from the regressions between SD_{avg} and maize plant count calculated using different cell sizes.

4.2.3 Combined flights

4.2.3.1 Linear regressions between number of plants and average standard deviation

Linear regressions between SD_{avg} and the number of maize plants in the training areas was calculated using all cell sizes. Regressions for the 0.4 and 0.8 m cell sizes are plotted in

figure 29. Circles represent training areas, excluding $T4_2$ (red square). The DVA and SVA areas from both flights are plotted for the 0.8 m cell size (blue triangles). Trend lines are fitted for the 0.8 m (R^2 = 0.68) and 0.4 m (R^2 = 0.54) resolutions, indicating a negative relationship between the two variables. An increasing trend of R^2 values with cell size can be noticed in figure 30, with large deviations from this trend at 0.55 and 0.85 m cell sizes. The regression using 0.95 m cell size resulted in the highest R^2 value (R^2 = 0.78), while using the 0.1 m cell size resulted in the lowest R^2 (R^2 = 0.42). Probability values (*p* values) are below the 0.05 significance level for all regressions except for three of the smaller cell sizes (Table 3), indicating a significant relationship between the number of plants and SD_{avg} for most regressions.

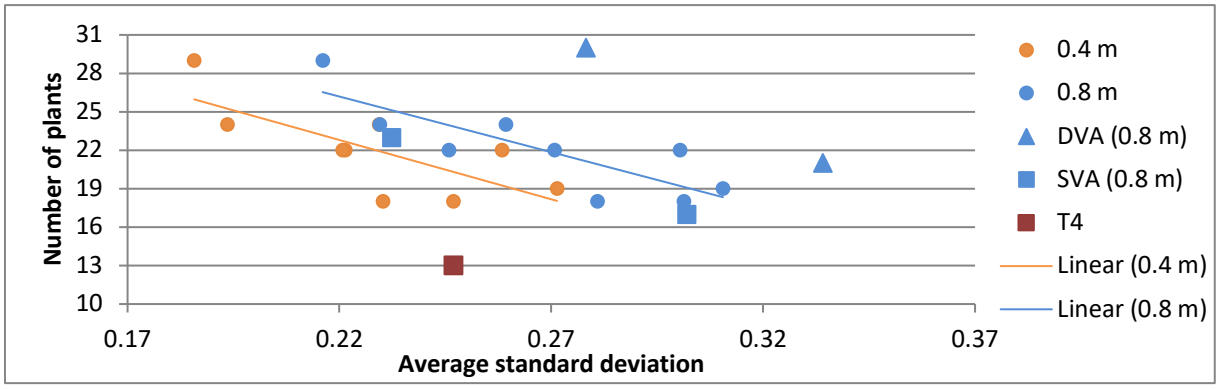

Figure 29. The estimated number of plants and the average standard deviation (SD_{avg}) is plotted for all training areas in both flights (excluding $T4_2$), for the 0.4 and 0.8 m cell sizes. The DVAs (triangles) and SVAs (blue squares) as well as $T4_2$ (red square) are plotted as reference. Trend lines indicate a negative relationship between the two variables.

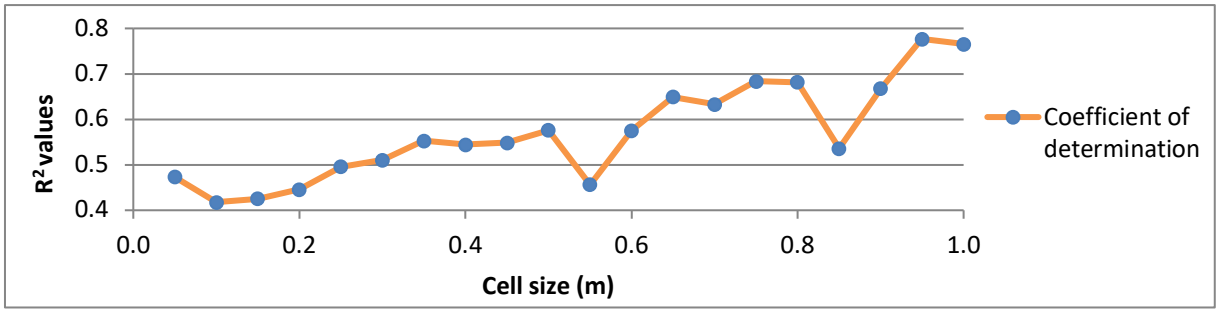

Figure 30. The blue circles represent the R^2 values of regressions between average standard deviation and the maize plant count. The regressions were calculated with different sampling cell sizes and all are presented here. The R^2 values increase slightly with cell size, but fluctuations from this trend can be noticed at 0.55 and at 0.85 m cell sizes.

Table 3. Probability-values (*p* values) shown for regressions made using different cell sizes. Probability values are seen to be below the 0.05 significance level for all regressions except those made with cell sizes of 0.1, 0.15 and 0.2 m.

Cell size	**0.05**	**0.1**	**0.15**	**0.2**	**0.25**	**0.3**	**0.35**	**0.4**	**0.45**	**0.5**
***p* value**	0.040	0.060	0.057	0.050	0.034	0.031	0.022	0.023	0.022	0.018
Cell size	**0.55**	**0.6**	**0.65**	**0.7**	**0.75**	**0.8**	**0.85**	**0.9**	**0.95**	**1**
***p* value**	0.046	0.018	0.009	0.010	0.006	0.006	0.025	0.007	0.002	0.002

4.2.3.2 Prediction of maize in validation areas

Maize plant density was predicted for the dense and sparse validation areas of both flights, using the equations from the regression of all training areas. The predictions of the SVAs (Fig. 31) were within one or two plants of the counted number of plants, with the predictions of SVA_1 being the most accurate. The predictions of both DVAs (Fig. 32) underestimated the number of plants. The accuracy of the predictions varied depending on the cell size used for the regressions, but no optimal cell size can be determined.

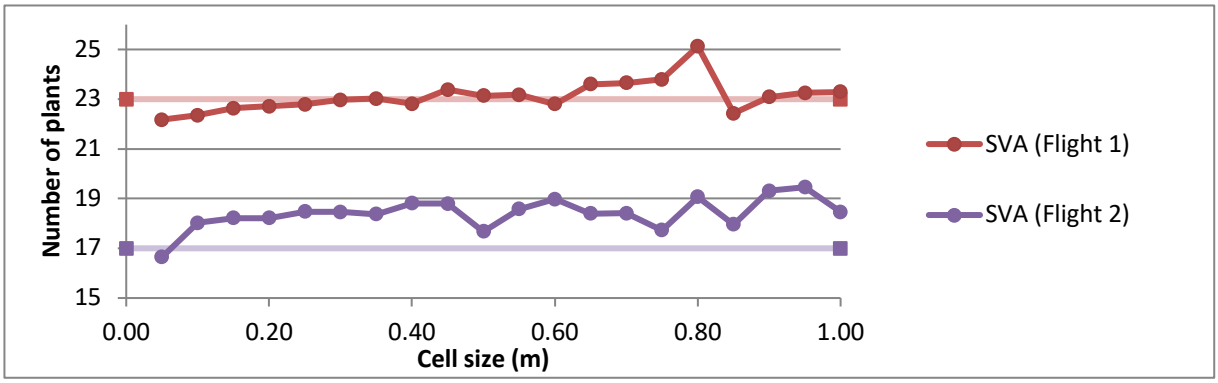

Figure 31. The prediction of maize density in the sparse validation area (SVA) for each flight, in comparison to the estimated plant number in each SVA. The predictions in the graph are based on the regression of all training areas using different cell sizes. The counted number of plants is seen as a straight line in reference to the predictions. The predictions can be seen to be within one or two plants of the counted number of plants.

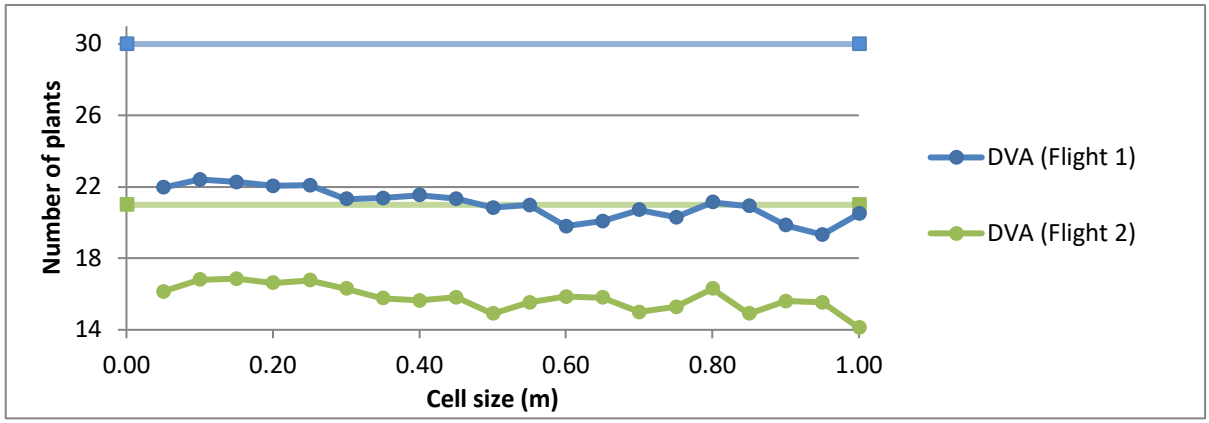

Figure 32. The prediction of maize in the dense validation area (DVA) of each flight, in comparison to the estimated plant number in each DVA. The predictions in the graph are based on the regression of all training areas using different cell sizes. The counted number of plants is seen as a straight line in reference to the predictions, with colors corresponding to the ones used for the predictions. The predicted number of plants is underestimated for both DVAs. DVA_1 was underestimated with between 7 and 11 plants, and DVA_2 with between 4 and 7 plants.

4.2.4 Exploration of outlying data samples

The DVA_1 in Flight 1 as well as $T4_2$ in Flight 2 displayed deviating SD_{avg} values in relation to plant density in comparison to other areas, and were therefore explored further.

The DVA_1 of Flight 1 displayed high standard deviation values in relation to the $T1_1$ area in the same flight, although both had similar maize plant counts (31, 29 plants). Upon closer examination, a large amount of low-lying points was detected in the western and northeastern part of this area (Fig. 33, (a)). These low-lying points corresponded with the location of areas of high standard deviation in the grids (Fig. 33, (b)). The ground is clearly visible between the maize plants in this area upon inspection of the orthomosaic, and the plants grow slightly further apart (Fig. 33, (b)).

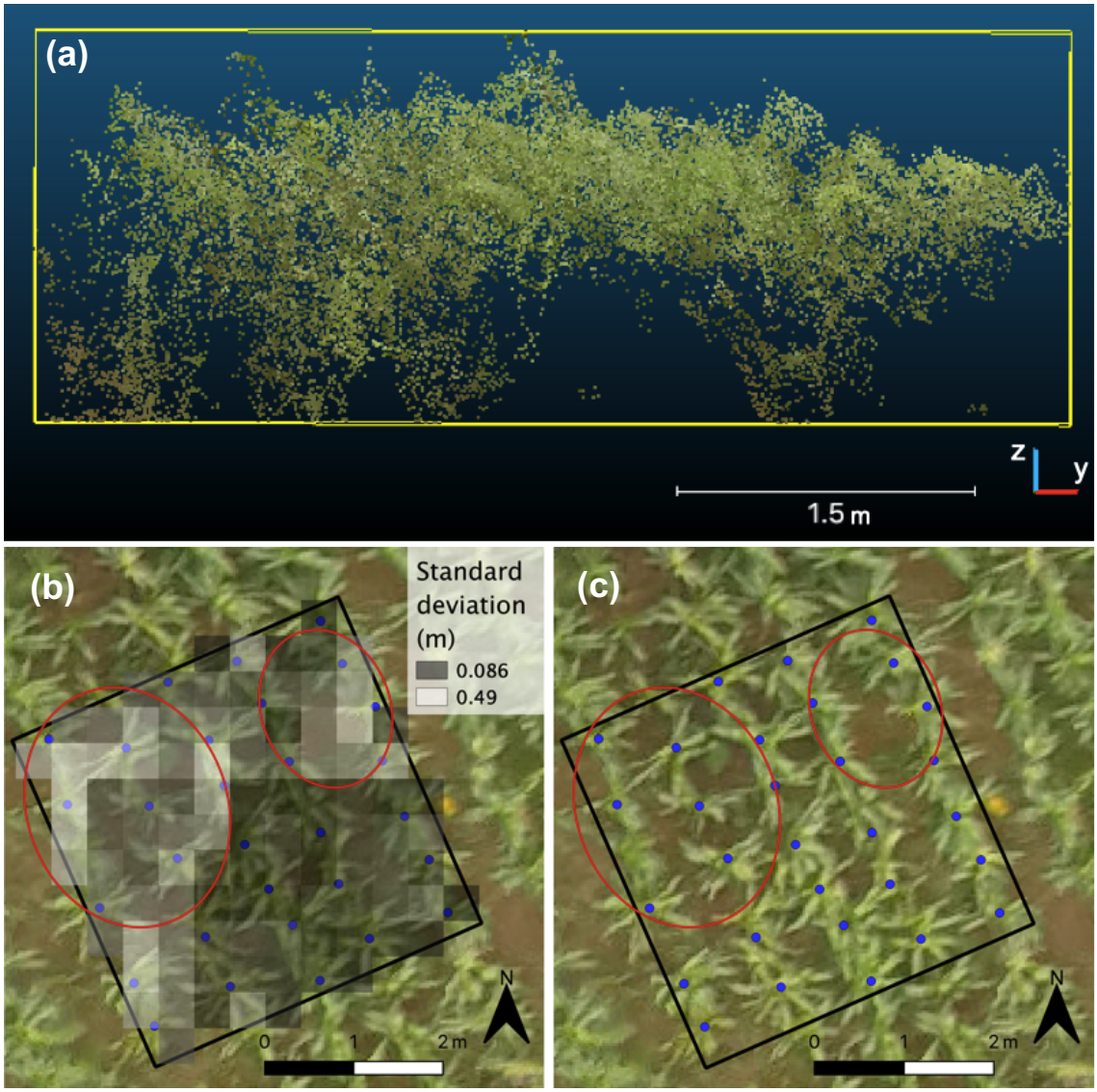

Figure 33. The top figure (a) shows the point cloud of the DVA_1 viewed horizontally from the south-eastern edge of the 4 x 4 m sample area. In (b) the same sample area (black square) is viewed from above, with a 0.4 x 0.4 m grid of standard deviation viewed on top of the orthomosaic. Brighter cells in the grid equal higher standard deviation values, and correspond to the areas of low-lying points in the top figure as well as areas of clearly visible ground in (c). (c) shows the DVA_1 sample area on top of the orthomosaic, with no grid overlaid.

A similar inspection of $T1_1$ also showed that higher standard deviation values corresponded to areas where the ground was clearly visible between maize plants (Fig. 34), however the standard deviation values are comparatively lower than for the DVA_1.

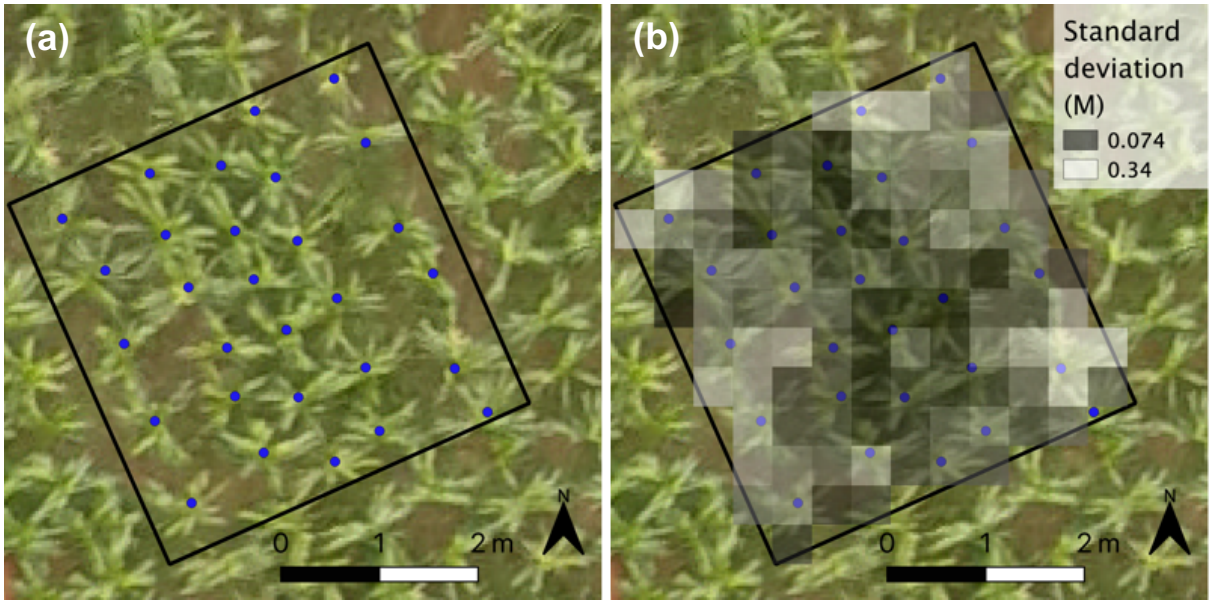

Figure 34. In (a), the estimated location of maize plants is shown on top of the orthomosaic within $T1_1$. In (b), a grid of standard deviations (0.4 x 0.4 m) is shown on top of the same sample area. The areas where the ground is visible between the maize plants in (a) correspond to areas of higher standard deviation (brighter cells) in (b).

$T4_2$ in Flight 2 displayed low standard deviation values in comparison to other areas in the same flight. As the area only had maize growing on one part of the field, it was omitted as an outlier from the regression analysis. Low standard deviation values corresponded to the area without maize plants (Fig. 35).

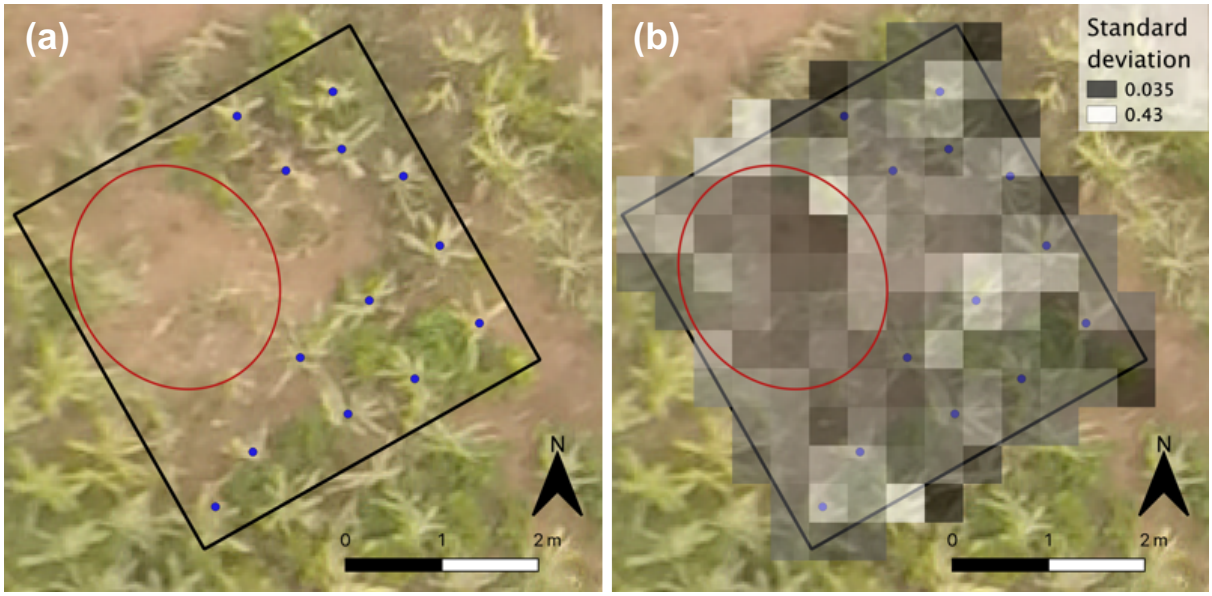

Figure 35. In (a), the $T4_2$ sample area is seen on top of the orthomosaic, with blue points corresponding to estimated maize plant positions. The left side of the area is seen to be almost completely without maize. This area corresponds to low standard deviations as seen in (b), where a grid of 0.4 x 0.4 m resolution is fitted on top of the orthomosaic. Darker cells indicate lower standard deviation values.

4.2.5 Field scale plant density estimation

The equation for the regression using 0.75 m cell size was used for estimating maize density in the AOI of flight 1, resulting in a plant density map on a field scale (Fig. 36, (a)). The map can be seen in relation to the orthophoto (Fig. 36, (b)), and a grid with 4 x 4 m cells is shown in the map where brighter cells indicates lower plant density. The dark area in the northern part of the grid indicates high plant density, and seems to correspond well with an area of densely growing maize as seen in the orthophoto. The brighter cells on the eastern side of the grid indicate areas of lower plant density, and correspond with an area of sparse growing maize on the orthophoto. The edges of the maize field, such as the north-west corner by the road, and the south-east corner, are estimated as areas of low plant density. This is likely since height contrasts between maize and bare ground resulted in high standard deviations. The same phenomenon can be seen for the south-western area, where a large tree and a group of smaller trees likely generated large variations in point heights in the point cloud.

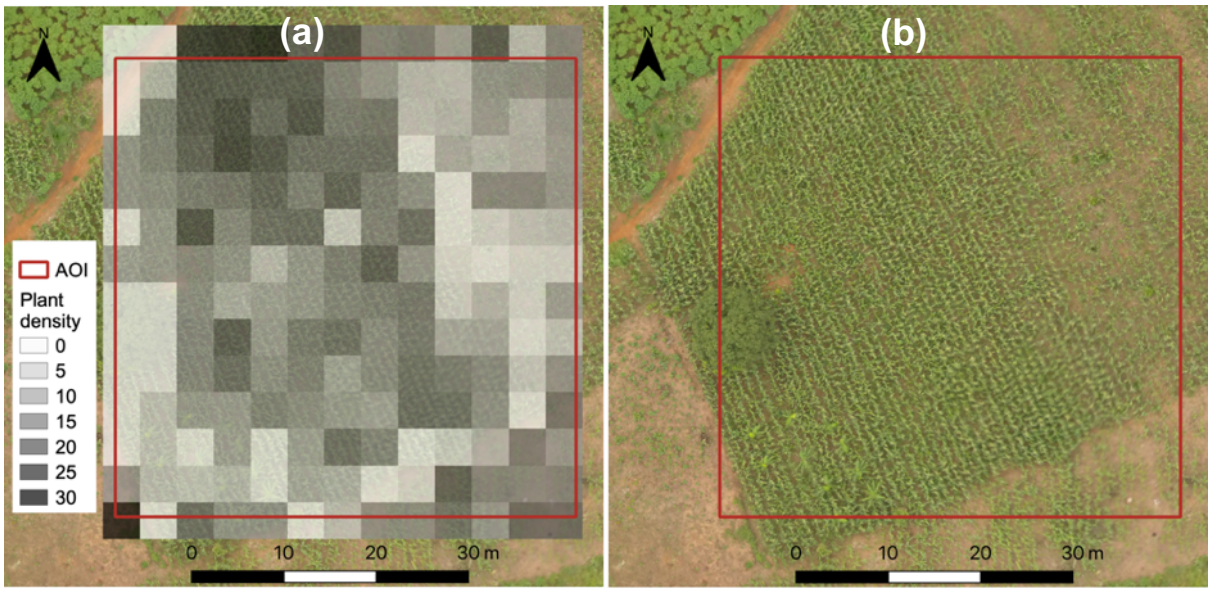

Figure 36. (a) shows a grid of estimated plant density based on standard deviation values within 4 x 4 m cells in the AOI of Flight 1. The cell values were calculated using an equation from the regression where the average standard deviation of the training areas had been calculated using a grid of 0.75 x 0.75 m cell sizes. The same AOI on top of an orthomosaic is shown in (b) without a grid overlaid. Areas of low plant density are represented by brighter cells and correspond to an area on the right-hand side of the orthomosaic as well as along the edges of the field and the south-western corner where a group of trees are located. An area in the north has darker cells that indicate dense growing maize, and this corresponds to an area of densely growing maize in the orthophoto.

4.3 Method 2: Detecting maize plants from elevation contours

As the results for Flight 1 and Flight 1 yielded results of similar characteristics with this method, only the results for Flight 1 are presented here. Results for Flight 2 can be seen in Appendix E.

The contour lines were generated with 0.1m Z-value intervals and the contours were queried to contain lines of lengths between 0.2 and 3.0 m, on elevations minimum 1.0 m below the highest point in the validation area. The contour locations correspond to the estimated locations of the maize plants (blue dots) to some extent for both the DVA_1 and the SVA_1 (Fig. 37). However, many contours are found in places that do not contain a maize plant according to the estimated maize plant positions. The contour filtering for SVA_1 resulted in a somewhat larger number of estimated maize plant locations with no associated contours.

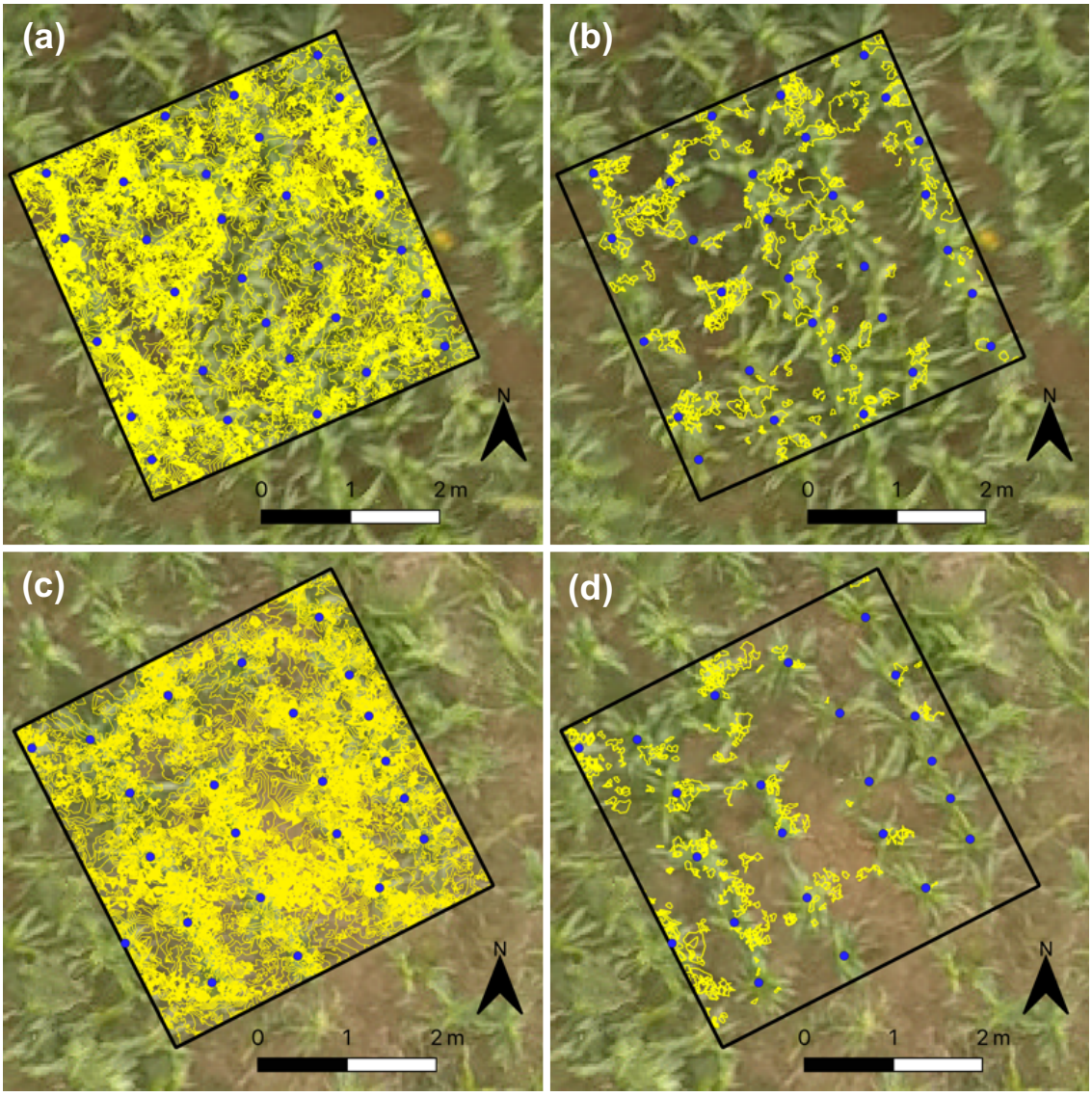

Figure 37. The location of all contour lines (yellow lines) within the DVA_1 (black square) is shown in (a). In (b), the remaining contours after the filtering on height and length in the DVA_1 is shown. Maize plant locations estimated from the orthomosaic are shown as blue points as a reference. In (c) and (d), the same information is shown for the SVA_1.

5 Discussion

5.1 Data quality

Blurry imagery due to displacement of the UAV camera during flight is known to impact the accuracy of plant height estimation (Han et al. 2018), the amount of features detected in the image, their correct positioning and the matching of features between photos in the bundle adjustment process (Sieberth et al. 2015) and might therefore have influenced the results of the two methods. The point clouds of the sampled training and validation areas contained differing amounts of points (Table 1 and 2), and the sample areas of Flight 2 had generally lower point counts than the sample areas of Flight 1. As the imagery of Flight 2 were deemed to be blurrier, this might indeed be attributed to the varying ability of feature identification algorithms to identify image features due to differences in blur and light conditions both within and between the two flights.

Furthermore, the data was not gathered with 3D modelling in mind, and consequently did not employ an optimal flight planning for this purpose. The one-directional flight pattern used in this case might have hindered optimal quality of the produced point clouds in comparison to also including data gathered from a flight perpendicular to the first direction (De Souza et al. 2017).

5.2 Method 1: Detecting maize plant density from canopy structure

Li et al. and Mathews and Jensen, have previously attempted to estimate LAI through metrics of the canopy structure of crops. Similar to this, the first method of this study aimed to explore whether a metric of canopy structure could be used to estimate maize plant density. The metric of canopy structure used in this study was the SD_{avg} of point heights within an area. The second research question of this study regarded finding an optimal sampling unit size for this metric. For this reason, the SD_{avg} was calculated for twenty different grids with different sampling unit sizes, or cell sizes, in each sample area. In these grids, the cell values corresponded to the standard deviation of point height in the sample area point cloud (Fig. 10).

By plotting the SD_{avg} versus grid cell size for the sample areas (Fig. 18 and 23), a general increase of SD_{avg} with larger cell sizes could be noticed. This was expected, as the points are more likely to be of similar elevation the closer they are to each other. Furthermore, the SD_{avg} fluctuated slightly after approximately 0.6 m cell sizes, and considerably after 0.8 m cell sizes. This was likely due to variations in the positioning of the cells within the 4 x 4 m sample areas. Since the training areas were aligned along the row direction of the maize field rather than north-south aligned, larger grid cells left triangular gaps that differed between cell sizes, meaning different parts of the area was covered depending on the cell size. To avoid these edge effects, the sampling cell size should therefore not be too large.

The coefficient of determination (R^2 values) varied with the cell size used to sample standard deviation values for the regression equation, and the cell size used for the regression giving the best R^2 values varied between Flight 1, Flight 2 and the combined flight (Fig. 20, 26 and 30). No optimal cell size could therefore be determined. However, regressions using grids with the smallest cell sizes generally made for lower R^2 values. Again, this is likely due the fact that points closer to each other have similar elevation values, and the smallest cell sizes might therefore be inadequate for capturing point variance. Resolutions of 0.8 m and lower showed a somewhat higher fluctuation in R^2 values. However, when visually inspecting the graphs of R2 values in all three cases, an overarching trend of higher R^2 values with lower resolutions could be noticed. The regressions using 0.6, 0.7 and 0.8 m cell sizes had relatively high R^2 values in all cases, pointing to relatively large cell sizes being preferable for the method. This might be because larger cell sizes better captured variations in the canopy structure. In response to RQ2, no optimal sampling unit size could be concluded, but using cell sizes between approximately 0.6 and 0.8 might be suitable for this particular sampling method.

In line with the assumption (Fig. 5), a pattern of lower standard deviations for sample areas with higher plant count was noticed. This held true especially for Flight 1, where only the DVA_1 deviated from this trend (Fig. 18). For the sample areas of Flight 2 (Fig. 23), deviations from this trend could be seen for the DVA_2 and $T4_2$. The histograms of point distributions (Fig. 16 and 17) gave clues to two issues related to the trend deviations in these areas.

Firstly, the point distributions could be seen to align with the maize density in the respective areas to some extent, with more concentrated point distributions for areas of higher density. However, some areas deviated from this. The DVAs in both flights had a slightly broader frequency distribution than expected, as well as standard deviations closer to those of sparser areas. Further exploring the DVA_1 of Flight 1, a high amount of points on low elevations were identified in two areas of the point cloud where more ground was seen between plants (Fig. 33). This increased SD_{avg} and made for a broader point distribution within the area. These results are in line with the assumption outlined in section 3.3.1 (Fig. 5), but simultaneously points to vulnerability of the method with regards to variations in plant density within sample areas.

The second issue noticed was the skewed distributions of points at different elevation within the areas. The histograms of some sample areas showed a presence of a few points on high elevations (See $T1_2$, Fig. 16), causing long right-hand tails on the graphs. A Z threshold of 2 m from the highest located point was applied to all areas to remove low lying noise, but due to the presence of these few highly located points, this threshold might have cut off low lying points that were correctly placed. This could have affected the derived standard deviations and consequently the accuracy of the regression analysis. However, it is also possible that part of the points on the tail belonged to maize tassels stretching above the bulk of other features in the canopy. Removing highly located points was therefore considered risky, especially since the elevation contour analysis could be assisted by the detection of maize plant tassels. A Z threshold based on a georeferenced ground surface would have

removed low lying noise points while ensuring that no relevant points were removed. Such an improvement should be considered in a future study.

The $T4_2$ of Flight 2 displayed a broad point distribution in accordance with its low plant density (Fig. 18). However, the SD_{avg} of this area was considerably lower than other areas of sparse density. This was likely due to the fact that the plot had a large area of bare ground in one part of the field (Fig. 35) and the low elevation variations of the bare ground area lowered the SD_{avg}. Similar to the issues mentioned with the standard deviation of the DVAs, this point to vulnerability of this method with regards to varying plant densities within sample areas. It can be reasonable to assume that the methods would not work for areas that are not covered with maize plants of some density or another, and the $T4_2$ area was omitted from the regression analysis.

However, the $T4_2$ area pointed to an important issue that arises upon upscaling this method for an entire field. If the density of a whole maize field is estimated section by section, the resulting standard deviations could be similar for a section with bare ground and a section with densely growing maize. Patches of bare ground is a likely scenario for smallholder maize farmers, and could result in misleading density-estimations with this method.

Despite potential differences between Flight 1 and 2 regarding point cloud quality, maize heights, and plant spatial distribution, the regression from using training areas from both flights indicated a negative relationship between plant density and SD_{avg}. This indicated that the results from both fields were consistent in the relation between the two variables. Predictions based on the regression of all training samples resulted in predictions similar or slightly better than the ones from the flights separately (Fig. 31 and 32). The predictions of the validation area with the highest accuracy were around 22 to 23 plants where 23 plants had been counted (Fig. 31). The predictions of the validation area with the lowest accuracy were between 19 and 22 plants where 30 plants had been counted (Fig. 32). This can be put into relation to Hall et al., who estimated 663 maize plants where 553 were counted (overestimation of 15%) using an object oriented image classification on maize fields in a similar environment (2018).

Method 1 was finally used to predict maize densities on a field scale, using the point cloud of the AOI of Flight 1. The regression equation using a 0.75 m cell size was used for predicting plant density, since it had high R^2 and low p values and was in the range of reasonable cell sizes as discussed earlier. The final result was a map of predicted maize plant density per 4 x 4 m cell (Fig. 36). When compared to the orthomosaic of the same area, the map could be seen to indicate densely growing areas as areas of high plant density, and vice versa. The field-level predictions likely did not give the true maize count, but showed that the standard deviation of the canopy structure in an area can to some extent indicate plant density. In answer to RQ1, the results were likely not accurate enough to indicate plant density on a level of detail suitable for precision agriculture purposes, but could possibly be used to improve yield forecasting models together with complementary data sets. R2 values and p values together indicated a relationship between canopy structure and plant density. The significance-level was set at 0.05, and all regressions except the ones using 0.1, 0.15 and 0.2 sampling cell sizes (table 3) were statistically significant. However, it should be

emphasized that the data sample size in this exploratory study was too small to draw a strong conclusion of statistical significance between these variables.
Furthermore, the predictions of maize density in the validation areas were of widely varying accuracy. The varying predictions were likely related to the variations in spatial distribution of plants inside the 4 x 4 m sample areas. One area can have the same amount of plants as another area, but if the spatial distribution of maize plants varies between the areas, the canopy structures modelled by the point cloud will differ. Since the SD_{avg} is a metric based on the canopy structure, this results in different SD_{avg} values in areas of the same plant count. This also means that if the maize plant distribution varies greatly over small distances without a clear pattern, the method is less likely to be accurate.

The success of method 1 is therefore likely impacted by the spatial pattern of plants in maize field being modelled. Furthermore, the sample area size utilized is likely to be more or less suitable depending on the spatial distribution of maize. Using smaller sample areas could possibly lead to a more homogenous maize distribution within a single area, depending on the gradient of change at which maize plant density differs within a field. However, larger sample areas could also potentially mitigate the effect of varying plant distribution. If the canopy structure is averaged in a larger sample area, variations in plant distribution within the area might have a smaller impact overall. If the sample area is too small, variations in plant distributions risk leading to larger spreads in standard deviations for areas with similar plant counts.

As the sample size of this study was small, a future study should include a larger sample to enable greater certainty of the results. Apart from using a larger sample size, a future study should also explore the impact of different sample area sizes for using this method in a similar growing environment. Furthermore, such a study should also employ optimal data gathering practices with regards to flight pattern as well as less blurry imagery. A future study can also further evaluate the accuracy of this method by comparing the field maize density map (Fig. 36) to validation data on maize plant density in larger areas sampled in the field.

5.3 Method 2: Detecting maize plants from elevation contours

The transects of the maize field point clouds showed peaks and valleys along the transect lines that represented maize plants (Fig. 14 and 15), and this indicated the possibility of generating elevation contours that would delineate individual plants. An initial assumption was that setting a maximum length of the contour would be enough to delineate the smaller tops that would represent the center-located maize plant tassels. However, this generated many smaller contours in places where likely no maize plants were positioned. The next attempt utilized both a minimum Z value and an interval of contour lengths which was believed to be long enough not to encompass small and scatter contours, but small enough to exclude all contour lines that connected larger areas between the maize plants. This generated a collection of contours in the vicinity of every maize plant, but did not generate a result of clearly-defined contours on positions close to the maize plants estimated center (Fig. 37).

The maize plants tassels constitute the center of the maize plants, but might have been too small in relation to the resolution of the imagery used in this study to be identified as image features. Instead, a collection of top leaves sticking out in different directions likely provided multiple peaks for individual maize plants. Furthermore, if the maize plants are of differing heights, contour lines generated on a certain elevation might capture one plant but not another. These contours were therefore difficult to trust and use as a reference for the location of individual maize plants. However, the locations of maize plants were estimated remotely from orthomosaics, and the height was estimated from field data of subplots in the vicinity. Therefore, the accuracy of the results could not be precisely determined. Validation data on the location and height of the plants would have been greatly beneficial in determining values for querying contours, and helped quantify the impact of data quality on the results.

6 Conclusions

The increasing need for resource-efficient food production is highlighted by an increasing global population, with the largest projected population increase on the African continent. Crop monitoring with remote sensing could contribute both to furthering crop productivity in smallholder farmers and be used for yield forecasting. In light of this, two methods for crop monitoring of agricultural smallholder farm fields in Ghana were tested in this study. The two explored methods utilized SfM point clouds in attempts to estimate maize plant density, an important crop parameter related to yield. The first method explored a potential relationship between a metric of variations in canopy structure and maize plant density. The results of this method indicated a relationship between the two variables, and might therefore have potential for providing indications of variations of maize plant density within a field. However, it should be emphasized that the sample size of this exploratory study was too small to draw a conclusion of a statistical relationship between the two variables. Furthermore, the method proved vulnerable with regards to the presence of larger areas of bare ground as well as heterogeneity of the plants distribution within the sample area. A future study should therefore utilize a larger sample, mask out large areas of bare ground before applying the method, as well as explore different sample area sizes to potentially mitigate the impact of heterogeneous plant distributions.

The second method attempted to locate individual maize plants through an elevation contour analysis. This method produced results of low accuracy, as the contours did not consistently align with the estimated location of the maize plants. The lack of a clearly definable center-point in the maize plants likely led to scattered contours, making it difficult to outline individual plants. Differing maize heights within an area also makes it hard to capture the top of individual maize plants. The method is therefore likely inadequate for locating objects with a complicated geometry such as maize plants.

In addition, the results were likely influenced by poor data quality. The accuracy of the point clouds might have been lowered due to varying light conditions during flight, image blurriness (Sieberth et al. 2014; Dandois et al. 2015) as well as suboptimal flight planning (De Souza et al. 2017). This could have resulted in incorrectly placed low, or high lying points. However, due to a lack of validation data, the influence of data quality could not be determined on either method.

Nevertheless, the potential of relatively low cost methods based on SfM point clouds motivate further exploration in this field. Apart from revising the methods according to the previous discussion, future studies should consider stable light conditions and employ state of the art UAV flight planning for gathering data for constructing SfM point clouds. Additionally, validation data of the height and location of maize plants should be employed to assess accuracy of the SfM point clouds and better outline the viability and shortcomings of these SfM based methods.

7 References

Adu, G., M. . Abdulai, H. Alidu, S. K Nustugah, S. Buah, J. Kombiok, K. Obeng-Antwi, M. Abudulai, et al. 2014. *Recommended Production Practices for Maize in Ghana.* doi:10.13140/2.1.4376.3527.

Agisoft LLC. 2018. Agisoft PhotoScan. *Professional Edition, Version 1.2*. St. Petersburg, Russia.

Agribotix. 2018. Agribotix. Colorado: Agribotix.

Assefa, Y., P. Carter, M. Hinds, G. Bhalla, R. Schon, M. Jeschke, S. Paszkiewicz, S. Smith, et al. 2018. Analysis of Long Term Study Indicates Both Agronomic Optimal Plant Density and Increase Maize Yield per Plant Contributed to Yield Gain. *Scientific Reports* 8. Springer US: 1–11. doi:10.1038/s41598-018-23362-x.

Bai, Z., D. L. Dent, L. Olsson, and M. E. Schaepman. 2008. *Global assessment of land degradation and improvement 1: identification by remote sensing*. *Report 2008/01, FAO/ISRIC-Rome/Wageningen*.

Bendig, J., A. Bolten, and G. Bareth. 2013. UAV-based Imaging for Multi-Temporal, very high Resolution Crop Surface Models to monitor Crop Growth Variability
Monitoring des Pflanzenwachstums mit Hilfe multitemporaler und hoch auflösender Oberflächenmodelle von Getreidebeständen auf Basis v. *Photogrammetrie - Fernerkundung - Geoinformation* 2013: 551–562. doi:10.1127/1432-8364/2013/0200.

Bendig, J., K. Yu, H. Aasen, A. Bolten, S. Bennertz, J. Broscheit, M. L. Gnyp, and G. Bareth. 2015. Combining UAV-based plant height from crop surface models, visible, and near infrared vegetation indices for biomass monitoring in barley. *International Journal of Applied Earth Observation and Geoinformation* 39. Elsevier B.V.: 79–87. doi:10.1016/j.jag.2015.02.012.

Chen, Wei, X. Hu, Wen Chen, Y. Hong, and M. Yang. 2018. Airborne LiDAR remote sensing for individual tree forest inventory using trunk detection-aided mean shift clustering techniques. *Remote Sensing* 10: 1–25. doi:10.3390/rs10071078.

Ciampitti, I. A., and T. J. Vyn. 2011. A comprehensive study of plant density consequences on nitrogen uptake dynamics of maize plants from vegetative to reproductive stages. *Field Crops Research* 121: 2–18. doi:10.1016/j.fcr.2010.10.009.

CloudCompare. 2019. Cloud Compare.

Dandois, J. P., M. Olano, and E. C. Ellis. 2015. Optimal altitude, overlap, and weather conditions for computer vision uav estimates of forest structure. *Remote Sensing* 7: 13895–13920. doi:10.3390/rs71013895.

Daughtry, C. S. T., C. L. Walthall, M. S. Kim, E. B. De Colstoun, and J. E. McMurtrey. 2000. Estimating corn leaf chlorophyll concentration from leaf and canopy reflectance. *Remote Sensing of Environment* 74: 229–239. doi:10.1016/S0034-4257(00)00113-9.

Delincé, J. 2017. *Recent practices and advances for AMIS crop yield forecasting at farm and parcel level: A review*. Rome: FAO – AMIS Publication.

Delrue, J., L. Bydekerke, H. Eerens, S. Gilliams, I. Piccard, and E. Swinnen. 2013. Crop mapping in countries with small-scale farming: A case study for West Shewa, Ethiopia. *International Journal of Remote Sensing* 34: 2566–2582. doi:10.1080/01431161.2012.747016.

Dominique, C., D. Valérie, G. Martine, L. P. Michel, S. Vincent, F. Sylvain, and V. Amanda. 2016. Contribution of Remote Sensing for Crop and Water Monitoring. In *Land Surface Remote Sensing in Agriculture and Forest*, 113–177. doi:10.1016/B978-1-78548-103-1.50004-2.

Du, M., and N. Noguchi. 2017. Monitoring of wheat growth status and mapping of wheat yield's within-field spatial variations using color images acquired from UAV-camera System. *Remote Sensing* 9. doi:10.3390/rs9030289.

Duan, B., S. Fang, R. Zhu, X. Wu, S. Wang, Y. Gong, and Y. Peng. 2019. Remote Estimation of Rice Yield With Unmanned Aerial Vehicle (UAV) Data and Spectral Mixture Analysis. *Frontiers in Plant Science* 10: 1–14. doi:10.3389/fpls.2019.00204.

FAO. 2007. MOZAMBIQUE: Current Reform Completion. *Africa Research Bulletin: Economic, Financial and Technical Series* 43: 17222C-17222C. doi:10.1111/j.1467-6346.2007.00685.x.

FAO. 2017. *Sustainable Management of the Fall Armyworm in Africa FAO Programme for Action*.

Frey, J., K. Kovach, S. Stemmler, and B. Koch. 2018. UAV photogrammetry of forests as a vulnerable process. A sensitivity analysis for a structure from motion RGB-image pipeline. *Remote Sensing* 10.

doi:10.3390/rs10060912.

Geipel, J., J. Link, and W. Claupein. 2014. Combined spectral and spatial modeling of corn yield based on aerial images and crop surface models acquired with an unmanned aircraft system. *Remote Sensing* 6: 10335–10355. doi:10.3390/rs61110335.

Gnädinger, F., and U. Schmidhalter. 2017. Digital counts of maize plants by Unmanned Aerial Vehicles (UAVs). *Remote Sensing* 9. doi:10.3390/rs9060544.

Hall, O., S. Dahlin, H. Marstorp, M. Archila Bustos, I. Öborn, and M. Jirström. 2018. Classification of Maize in Complex Smallholder Farming Systems Using UAV Imagery. *Drones* 2: 22. doi:10.3390/drones2030022.

Han, X., J. A. Thomasson, G. C. Bagnall, N. A. Pugh, D. W. Horne, W. L. Rooney, J. Jung, A. Chang, et al. 2018. Measurement and Calibration of Plant-Height from Fixed-Wing UAV Images. *Sensors* 18: 4092. doi:10.3390/s18124092.

Harvey, P. 2019. ExifTool. Retreived from: https://exiftool.org/

He, F., T. Zhou, W. Xiong, S. M. Hasheminnasab, and A. Habib. 2018. Automated aerial triangulation for UAV-based mapping. *Remote Sensing* 10. doi:10.3390/rs10121952.

Höfle, B. 2014. Radiometric Correction of Terrestrial LiDAR Point Cloud Data for Individual Maize Plant Detection. *IEEE Geoscience and Remote Sensing Letters* 11: 94–98. doi:10.1109/LGRS.2013.2247022.

Hu, X., W. Chen, and W. Xu. 2017. Adaptive mean shift-based identification of individual trees using airborne LiDAR data. *Remote Sensing* 9: 1–24. doi:10.3390/rs9020148.

Hunt, E. R., and C. S. T. Daughtry. 2018. What good are unmanned aircraft systems for agricultural remote sensing and precision agriculture? *International Journal of Remote Sensing* 39. Taylor & Francis: 5345–5376. doi:10.1080/01431161.2017.1410300.

Isenburg, M. 2019. LAStools. Retreived from: https://rapidlasso.com/lastools/

van Ittersum, M. K., L. G. J. van Bussel, J. Wolf, P. Grassini, J. van Wart, N. Guilpart, L. Claessens, H. de Groot, et al. 2016. Can sub-Saharan Africa feed itself? *Proceedings of the National Academy of Sciences* 113: 14964–14969. doi:10.1073/pnas.1610359113.

Van Ittersum, M. K., K. G. Cassman, P. Grassini, J. Wolf, P. Tittonell, and Z. Hochman. 2013. Yield gap analysis with local to global relevance-A review. *Field Crops Research* 143. Elsevier B.V.: 4–17. doi:10.1016/j.fcr.2012.09.009.

Kihara, J., G. Nziguheba, S. Zingore, A. Coulibaly, A. Esilaba, V. Kabambe, S. Njoroge, C. Palm, et al. 2016. Understanding variability in crop response to fertilizer and amendments in sub-Saharan Africa. *Agriculture, Ecosystems and Environment* 229. Elsevier B.V.: 1–12. doi:10.1016/j.agee.2016.05.012.

Lambert, M. J., P. C. S. Traoré, X. Blaes, P. Baret, and P. Defourny. 2018. Estimating smallholder crops production at village level from Sentinel-2 time series in Mali's cotton belt. *Remote Sensing of Environment* 216. Elsevier: 647–657. doi:10.1016/j.rse.2018.06.036.

Lamm, F. R., R. M. Aiken, and A. A. A. Kheira. 2009. Corn Yield and Water Use Characteristics As Affected By Tillage, Plant Density, and Irrigation. *Transactions of the ASABE* 52: 133–143.

Li, W., Z. Niu, H. Chen, D. Li, M. Wu, and W. Zhao. 2016. Remote estimation of canopy height and aboveground biomass of maize using high-resolution stereo images from a low-cost unmanned aerial vehicle system. *Ecological Indicators* 67. Elsevier Ltd: 637–648. doi:10.1016/j.ecolind.2016.03.036.

Li, W., Z. Niu, H. Chen, and D. Li. 2017. Characterizing canopy structural complexity for the estimation of maize LAI based on ALS data and UAV stereo images. *International Journal of Remote Sensing* 38. Taylor & Francis: 2106–2116. doi:10.1080/01431161.2016.1235300.

Lowe, D. G. 2004. Distinctive Image Features from Scale-Invariant Keypoints. *International Journal of Computer Vision* 60: 91–110. doi:10.1023/B:VISI.0000029664.99615.94.

Madigan, E., Y. Guo, M. Pickering, A. Held, and X. Jia. 2018. QUANTITATIVE MONITORING OF COMPLETE RICE GROWING SEASONS USING SENTINEL 2 TIME SERIES IMAGES School of Engineering and Information Technology , The University of New South Wales , Canberra Campus , Canberra , ACT 2600 , Australia The CSIRO Land and Water : 7699–7702.

Magaia, E., S. Famba, I. Wesström, R. Brito, and A. Joel. 2017. Modelling maize yield response to plant density and water and nitrogen supply in a semi-arid region. *Field Crops Research* 205. Elsevier B.V.: 170–181. doi:10.1016/j.fcr.2016.12.025.

Maresma, Á., M. Ariza, E. Martínez, J. Lloveras, and J. A. Martínez-Casasnovas. 2016. Analysis of vegetation

indices to determine nitrogen application and yield prediction in maize (zea mays l.) from a standard uav service. *Remote Sensing* 8. doi:10.3390/rs8120973.

Marino, S., and A. Alvino. 2019. Detection of Spatial and Temporal Variability of Wheat Cultivars by High-Resolution Vegetation Indices. *Agronomy* 9: 226. doi:10.3390/agronomy9050226.

Mathews, A. J., and J. L. R. Jensen. 2013. Visualizing and quantifying vineyard canopy LAI using an unmanned aerial vehicle (UAV) collected high density structure from motion point cloud. *Remote Sensing* 5: 2164–2183. doi:10.3390/rs5052164.

Mensah, P., D. Katerere, S. Hachigonta, and A. Roodt. 2018. *Systems analysis approach for complex global challenges*. *Systems Analysis Approach for Complex Global Challenges*. Springer International Publishing. doi:10.1007/978-3-319-71486-8.

Michez, A., S. Bauwens, Y. Brostaux, M.-P. Hiel, S. Garré, P. Lejeune, and B. Dumont. 2018. How Far Can Consumer-Grade UAV RGB Imagery Describe Crop Production? A 3D and Multitemporal Modeling Approach Applied to Zea mays. *Remote Sensing* 10: 1798. doi:10.3390/rs10111798.

Molony, T., and J. Smith. 2017. Briefing: Biofuels, Food Security and Africa. *African Affairs* 109: 489–498. doi:10.1093/afratfadq019.

Mulla, D. J. 2013. Twenty five years of remote sensing in precision agriculture: Key advances and remaining knowledge gaps. *Biosystems Engineering* 114. IAgrE: 358–371. doi:10.1016/j.biosystemseng.2012.08.009.

Näsi, R., N. Viljanen, J. Kaivosoja, K. Alhonoja, T. Hakala, L. Markelin, and E. Honkavaara. 2018. Estimating biomass and nitrogen amount of barley and grass using UAV and aircraft based spectral and photogrammetric 3D features. *Remote Sensing* 10: 1–32. doi:10.3390/rs10071082.

Nellemann, C., and M. MacDevette. 2009. *The environmental food crisis : the environment's role in averting future food crisis : a UNEP rapid response assessment*. Arendal: UNEP/GRID-Arendal.

Ogola, J. B. O., T. R. Wheeler, and P. M. Harris. 2005. Water use of maize in response to planting density and irrigation. *South African Journal of Plant and Soil* 22: 116–121. doi:10.1080/02571862.2005.10634692.

Pasumansky, A. 2014. Agisoft web forum.

Pretty, J., and Z. P. Bharucha. 2014. Sustainable intensification in agricultural systems. *Annals of Botany*. doi:10.1093/aob/mcu205.

Qiu, Q., N. Sun, H. Bai, N. Wang, Z. Fan, Y. Wang, Z. Meng, B. Li, et al. 2019. Field-Based High-Throughput Phenotyping for Maize Plant Using 3D LiDAR Point Cloud Generated With a "Phenomobile." *Frontiers in Plant Science* 10: 1–15. doi:10.3389/fpls.2019.00554.

Rouse, J. W. J., R. H. Haas, and D. W. Deering. 1973. Monitoring Vegetation Systems in the Great Plains with ERTS. In *Third Earth Resources Technology Satellite-1 Symposium- Volume I: Technical Presentations. NASA SP-351*, 309–317.

Sangoi, L. 2001. Understanding Plant Density Effects on Maize Growth and Development: an Important Issue To Maximize Grain Yield a Compreensão Dos Efeitos Da Densidade De Plantas Sobre O Crescimento E Desenvolvimento Do Milho É Importante Para Maximizar O Rendimento De Gr. *Ciência Rural* 31: 159–168. doi:10.1590/S0103-84782001000100027.

Schonberger, J. L., and J.-M. Frahm. 2016. Structure-from-Motion Revisited: 4104–4113. doi:10.1109/cvpr.2016.445.

Semyonov, D. 2011. Agisoft web forum.

Shi, Y., N. Wang, R. K. Taylor, and W. R. Raun. 2015. Improvement of a ground-LiDAR-based corn plant population and spacing measurement system. *Computers and Electronics in Agriculture* 112. Elsevier B.V.: 92–101. doi:10.1016/j.compag.2014.11.026.

Sieberth, T., R. Wackrow, and J. H. Chandler. 2014. Influence of blur on feature matching and a geometric approach for photogrammetric deblurring. *International Archives of the Photogrammetry, Remote Sensing and Spatial Information Sciences - ISPRS Archives* 40: 321–326. doi:10.5194/isprsarchives-XL-3-321-2014.

Sieberth, T., R. Wackrow, and J. H. Chandler. 2015. UAV image blur-its influence and ways to correct it. *International Archives of the Photogrammetry, Remote Sensing and Spatial Information Sciences - ISPRS Archives* 40: 33–39. doi:10.5194/isprsarchives-XL-1-W4-33-2015.

Silva, P. R. F. da, M. L. Strieder, R. P. da S. Coser, L. Rambo, L. Sangoi, G. Argenta, E. L. Forsthofer, and A.

A. da Silva. 2006. Grain yield and kernel crude protein content increases of maize hybrids with late nitrogen side-dressing. *Scientia Agricola* 62: 487–492. doi:10.1590/s0103-90162005000500014.

Solomon, K. F., Y. Chauhan, and A. Zeppa. 2017. Risks of yield loss due to variation in optimum density for different maize genotypes under variable environmental conditions. *Journal of Agronomy and Crop Science* 203: 519–527. doi:10.1111/jac.12213.

De Souza, C. H. W., R. A. C. Lamparelli, J. V. Rocha, and P. S. G. Magalhães. 2017. Height estimation of sugarcane using an unmanned aerial system (UAS) based on structure from motion (SfM) point clouds. *International Journal of Remote Sensing* 38. Taylor & Francis: 2218–2230. doi:10.1080/01431161.2017.1285082.

United Nations. 2017. *World Population Prospects: The 2017 Revision, Key Findings and Advance Tables*. ESA/P/WP/248.

Vaccari, F. P., J. Primicerio, C. Belli, and A. Zaldei. 2015. Platforms for Precision Viticulture: 2971–2990. doi:10.3390/rs70302971.

Varela, S., P. R. Dhodda, W. H. Hsu, P. V. V. Prasad, Y. Assefa, N. R. Peralta, T. Griffin, A. Sharda, et al. 2018. Early-season stand count determination in Corn via integration of imagery from unmanned aerial systems (UAS) and supervised learning techniques. *Remote Sensing* 10. doi:10.3390/rs10020343.

van Vliet, J., D. A. Eitelberg, and P. H. Verburg. 2017. A global analysis of land take in cropland areas and production displacement from urbanization. *Global Environmental Change* 43. Elsevier Ltd: 107–115. doi:10.1016/j.gloenvcha.2017.02.001.

Wahab, I., O. Hall, and M. Jirström. 2018. Remote Sensing of Yields: Application of UAV Imagery-Derived NDVI for Estimating Maize Vigor and Yields in Complex Farming Systems in Sub-Saharan Africa. *Drones* 2: 28. doi:10.3390/drones2030028.

Wallace, L., A. Lucieer, Z. Malenovskỳ, D. Turner, and P. Vopěnka. 2016. Assessment of forest structure using two UAV techniques: A comparison of airborne laser scanning and structure from motion (SfM) point clouds. *Forests* 7: 1–16. doi:10.3390/f7030062.

Webb, N. P., N. A. Marshall, L. C. Stringer, M. S. Reed, A. Chappell, and J. E. Herrick. 2017. Land degradation and climate change: building climate resilience in agriculture. *Frontiers in Ecology and the Environment* 15: 450–459. doi:10.1002/fee.1530.

Westoby, M. J., J. Brasington, N. F. Glasser, M. J. Hambrey, and J. M. Reynolds. 2012. "Structure-from-Motion" photogrammetry: A low-cost, effective tool for geoscience applications. *Geomorphology* 179. Elsevier B.V.: 300–314. doi:10.1016/j.geomorph.2012.08.021.

Xue, J., and B. Su. 2017. Significant Remote Sensing Vegetation Indices : A Review of Developments and Applications 2017.

Yan, P., J. Pan, W. Zhang, J. Shi, X. Chen, and Z. Cui. 2017. A high plant density reduces the ability of maize to use soil nitrogen: 1–12. doi:10.1371/journal.pone.0172717.

Yizong Cheng. 2002. Mean shift, mode seeking, and clustering. *IEEE Transactions on Pattern Analysis and Machine Intelligence* 17: 790–799. doi:10.1109/34.400568.

Yoder, B. J., and R. E. Pettigrew-Crosby. 1995. Predicting Nitrogen and Chlorophyll Content and Concentrations from Reflectance Spectra (400-9 , 500 nm) at Leaf and Canopy Scales 4257: 199–211.

Zhang, C., and J. M. Kovacs. 2012. The application of small unmanned aerial systems for precision agriculture: A review. *Precision Agriculture* 13: 693–712. doi:10.1007/s11119-012-9274-5.

Zheng, J., W. N. Mmari, T. Nishigaki, M. M. Kilasara, and S. Funakawa. 2018. Nitrogen availability to maize as affected by fertilizer application and soil type in the Tanzanian highlands. *Nutrient Cycling in Agroecosystems* 112. Springer Netherlands: 197–213. doi:10.1007/s10705-018-9939-1.

Zhou, X., H. B. Zheng, X. Q. Xu, J. Y. He, X. K. Ge, X. Yao, T. Cheng, Y. Zhu, et al. 2017. Predicting grain yield in rice using multi-temporal vegetation indices from UAV-based multispectral and digital imagery. *ISPRS Journal of Photogrammetry and Remote Sensing* 130: 246–255. doi:10.1016/j.isprsjprs.2017.05.003.

8 Appendix A

Flight 1: Orthomosaic in Area of Interest

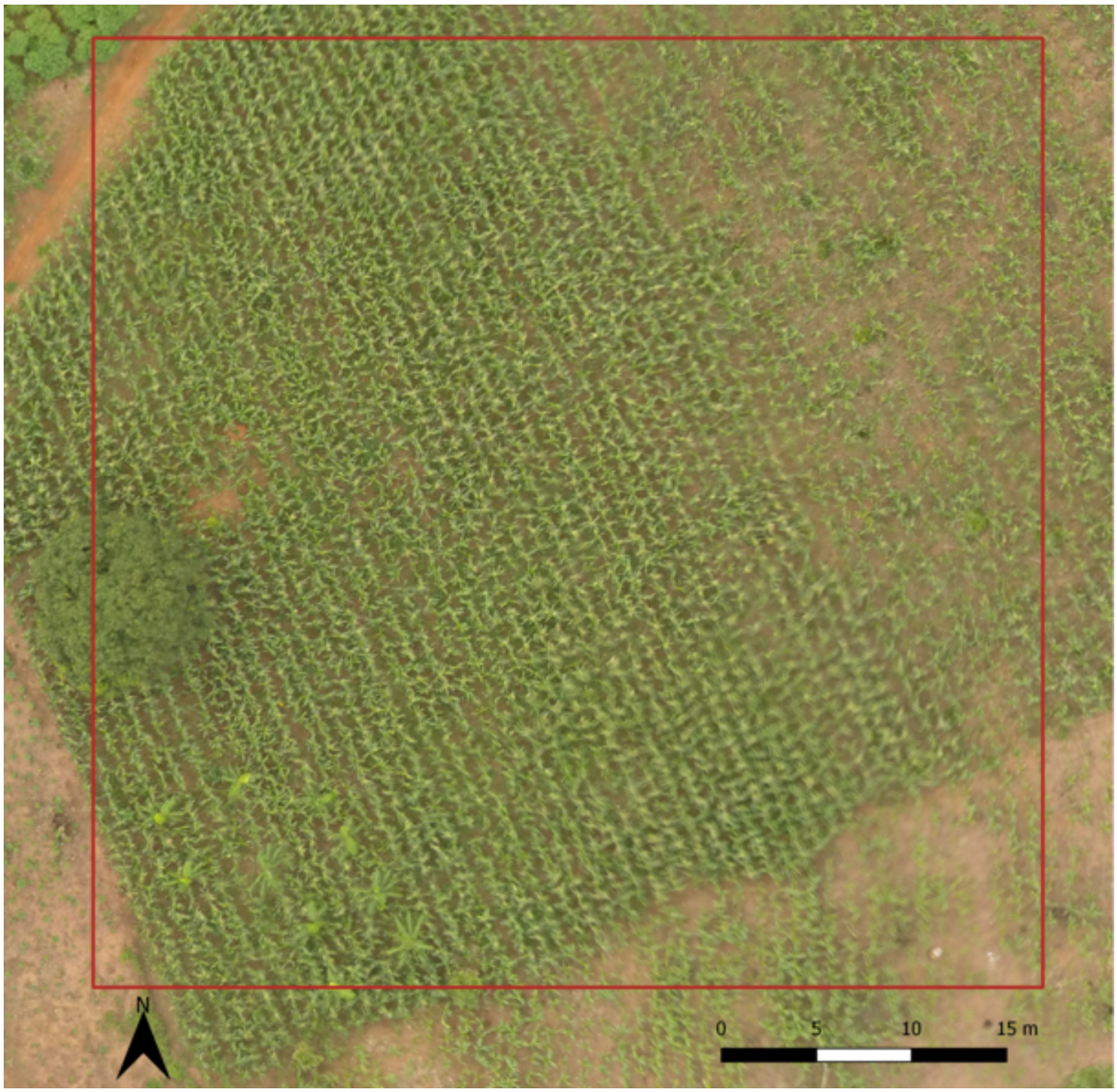

Figure 1. The Area of Interest (red rectangle) in which data was sampled for Flight 1, shown on top of the orthomosaic created from the drone imagery used in this study.

9 Appendix B

Flight 2: Orthomosaic, Area of Interest (AOI) 1

Figure 1. The Area of Interest (AOI) number 1, in which data was sampled for Flight 2 (blue rectangle). The AOI is shown on top of the orthomosaic created from the drone imagery used in this study.

10 Appendix C

Flight 2: Orthomosaic, Area of Interest 2

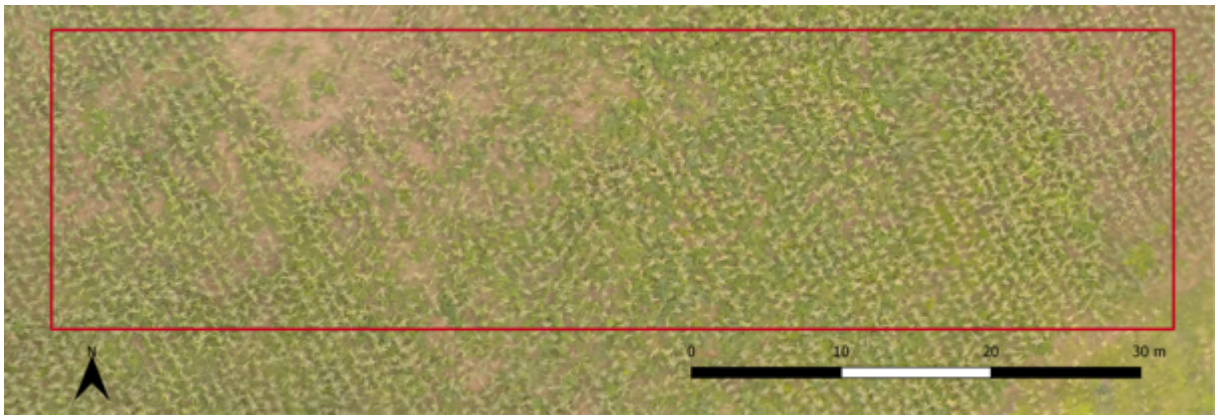

Figure 1. The Area of Interest (AOI) number 2, in which data was sampled for Flight 2 (red rectangle). The AOI is shown on top of the orthomosaic created from the drone imagery used in this study.

11 Appendix D

Flight 2: Areas of Interest and sample areas

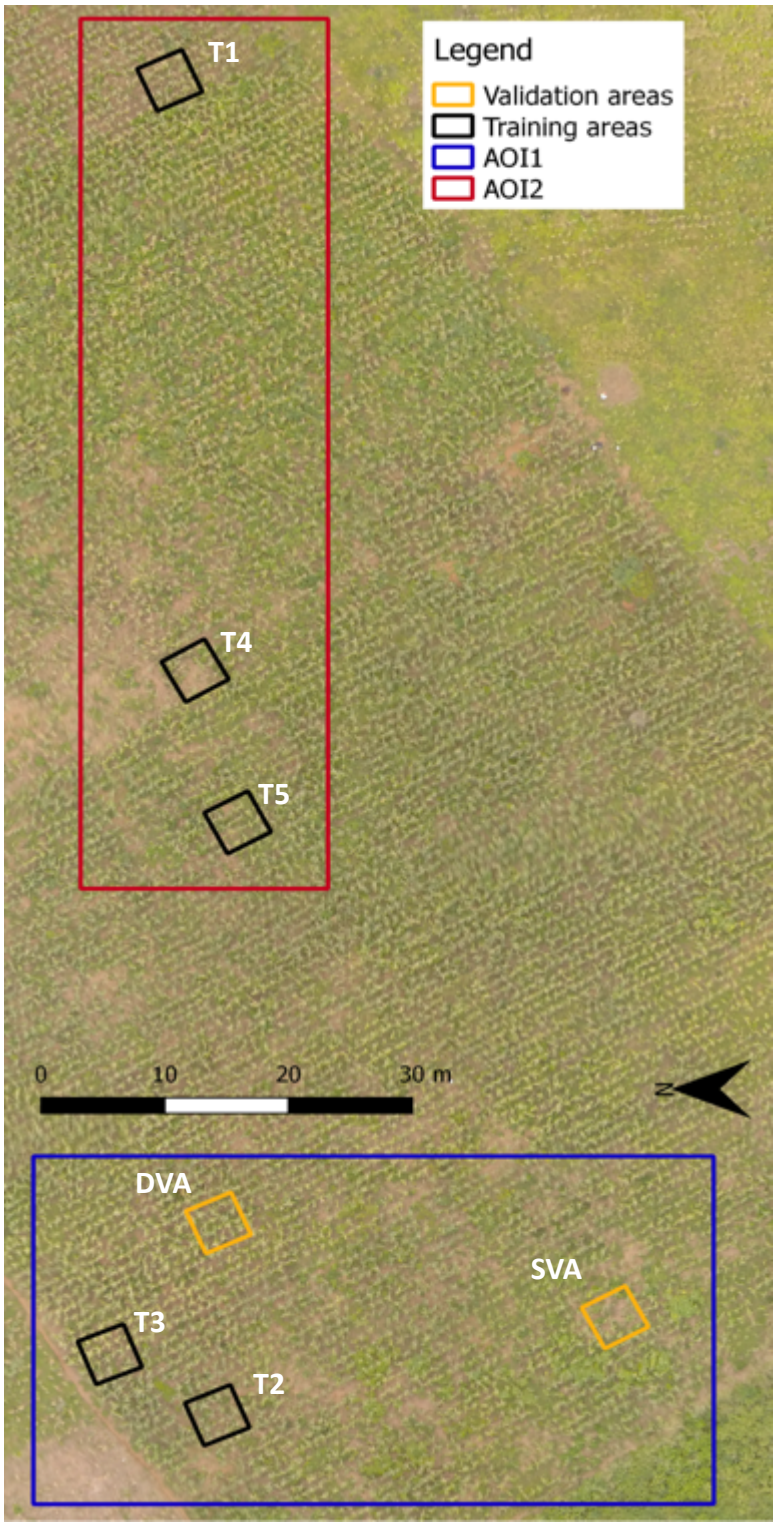

Figure 1. The two Areas of Interest (AOI) in which the sample was taken (red and blue rectangles), together with the total of 7 sample areas (black and yellow squares). The AOIs are shown on top of the orthomosaic created from the drone imagery used in this study.

12 Appendix E

Flight 2: Contour analysis for finding individual maize plants

The generated contours are located at some of the estimated maize plant locations for the DVA_2 (Fig. 1, (a) and (b)), however many contours are also found at locations not corresponding to the estimated locations. The contours for the SVA_2 are less accurately located, and fewer contours are found in the estimated locations of the maize plants (Fig. 1, (c) and (d)).

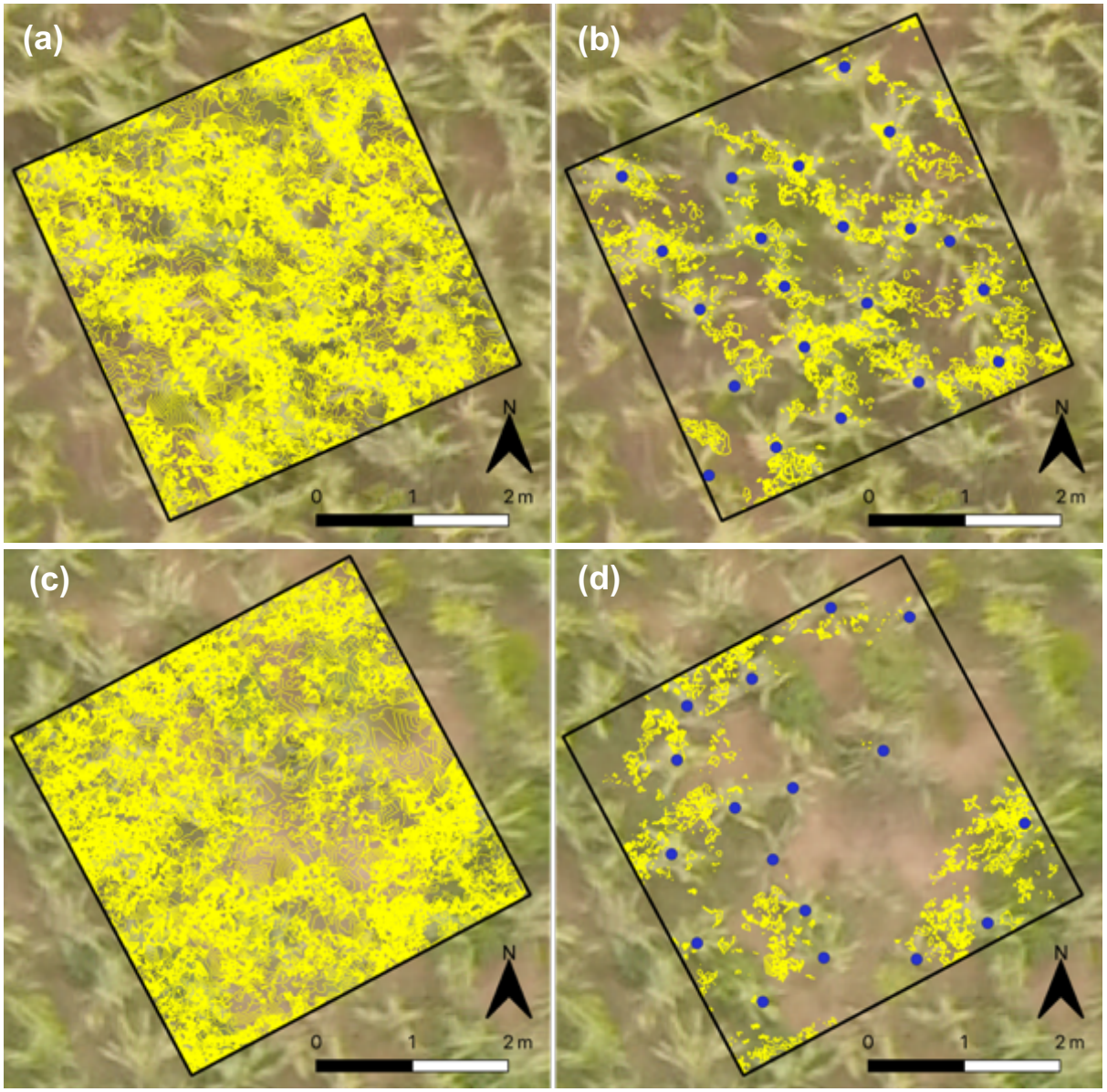

Figure 1. In (a), all generated height contours are shown for the DVA_2 (black square). In (b), the same sample area is shown but containing only the remaining contour lines after filtration on height and length. The same information of contour lines before filtering on height and length (c) and after filtering (d) for SVA_2. The estimated locations of the maize plants are shown as blue dots to be used in reference to the filtered contour lines.